

Middle-Late Jurassic to Early Cretaceous transtension and transpression during arc building in Central Chile: evidence from mafic dike swarms

Christian Creixell^{1*}, Miguel Ángel Parada¹, Diego Morata¹, Paulina Vásquez^{2*}, Carlos Pérez de Arce³, César Arriagada¹

¹ Departamento de Geología, Universidad de Chile, casilla 13518, Correo 21, Santiago, Chile.

cceixell@sernageomin.cl; maparada@cec.uchile.cl; dmorata@cec.uchile.cl; cearriagada@cec.uchile.cl

² Technische Universität Berlin, Fachgebiet Mineralogie-Petrologie, Sekr. ACK 9, Ackerstraße 71-79, 13355 Berlin, Germany.

pvasquez@sernageomin.cl

³ Laboratorio de Geocronología, Servicio Nacional de Geología y Minería, Tiltil 1993, Santiago, Chile.

cperezde@sernageomin.cl

* Present address: Servicio Nacional de Geología y Minería, Avenida Santa María 0104, Santiago, Chile. Phone: 56-2-4825500, Fax 56-2-7372026.

ABSTRACT. The Middle-Late Jurassic mafic dike swarms of central Chile between 33° and 33°45'S register the tectonic activity of the contemporaneous arc represented by the Coastal batholith. These dike swarms evidence alternate episodes of transtension and transpression across NW-striking structures, which controlled the construction of the magmatic arc. The Middle-Upper Jurassic and Lower Cretaceous mafic dike swarms in the Coastal range of central Chile has been studied through field observations, geochronology and AMS (anisotropy of magnetic susceptibility) to document the tectonic and magmatic evolution of the Jurassic-Cretaceous arc at this latitude. Middle to Upper Jurassic dike swarms (Concón and Cartagena mafic dike swarms) were emplaced between 163 and 157 Ma, along NW-SE to WNW-ESE-striking host fractures, registering a first stage of magma emplacement under sinistral transtension. During this stage, dikes acquired a fabric characterized by magnetic foliation clockwise oblique to dike trend and gently plunging lineations. This stage was followed rapidly by dike emplacement under sinistral transpression, with associated steeply plunging lineations in the dikes, reverse shear zones in the country rocks and local occurrence of horizontal mafic dikes. On the other hand, the Lower Cretaceous El Tabo Dike Swarm was emplaced along tensile fractures that do not register shear displacements along their walls. These dikes were emplaced at shallower crustal levels along tensile fractures. Within each dike swarm, differences in the tectonic style of emplacement correlates with changes in the geochemical composition of the dikes, suggesting a strong coupling between tectonics and nature of magma supplies in the arc. Finally, the current results show that the Mesozoic evolution of the Coastal Batholith of central Chile occurred in several stages of deformation and not under a simple scenario of extensional tectonics. This magmatism and deformation were strongly controlled by NW- to WNW-striking fractures. These structures are spatially correlated with regional-scale Cenozoic lineaments that are oblique to the orientation of the Andean orogen. We suggest that these lineaments are features inherited at least from Jurassic times.

Keywords: Dike swarm, Magma emplacement, Magnetic fabrics, Transtension, Transpression, Jurassic, NW-SE structures.

RESUMEN. Transtensión y transpresión del Jurásico Medio-Superior al Cretácico Inferior durante la construcción del arco magmático en Chile central: evidencia a partir de enjambres de diques máficos. Los enjambres de diques máficos del Jurásico Medio-Superior de Chile central entre los 33° y 33°45'S registran la actividad tectónica del arco contemporáneo representado por el batolito costero. Estos enjambres de diques evidencian episodios alternados de transtensión y transpresión a lo largo de estructuras de rumbo NW, las cuales controlaron la construcción del arco magmático. Los enjambres de diques máficos del Jurásico Medio-Superior y del Cretácico Inferior de la Cordillera de la Costa de Chile central han sido estudiados a través de observaciones de terreno, geocronología y Anisotropía de Susceptibilidad Magnética (ASM) para documentar la evolución tectónica y magmática del arco Jurásico-Cretácico en esta latitud. Los enjambres de diques del Jurásico Medio a Superior (enjambres de diques máficos de Concón y Cartagena) se emplazaron entre los 163 y 157 Ma, a lo largo de fracturas hospedantes de rumbo NW-SE a WNW-ESE, registrando una primera etapa de emplazamiento magmático bajo transtensión sinistral. Durante esta etapa, los diques adquirieron una fábrica caracterizada por foliación magnética oblicua en forma antihoraria respecto al rumbo de los diques y lineación de bajo ángulo. Esta etapa fue seguida rápidamente por emplazamiento de diques bajo transpresión sinistral, a la que se asocia lineaciones de alto ángulo en estos diques, zonas de cizalle inverso en las rocas de caja y ocurrencia local de diques máficos horizontales. Por otra parte, el enjambre de diques máficos de El Tabo fue emplazado a lo largo de fracturas de tensión que no registran desplazamientos a lo largo de sus paredes. Estos diques fueron emplazados en niveles corticales más superficiales gracias a fracturamiento extensional. Dentro de cada enjambre de diques, diferencias en el estilo tectónico de emplazamiento se correlaciona con cambios en la composición geoquímica de los diques, sugiriendo un fuerte acoplamiento entre la tectónica y la naturaleza de los magmas adicionados en el arco. Finalmente, estos resultados muestran que la evolución tectónica del batolito costero de Chile central ocurrió en varias etapas de deformación y no solo bajo un escenario simple de tectónica extensional. Este magmatismo y deformación fueron fuertemente controlados por fracturas de rumbo NW a WNW. Estas estructuras están espacialmente correlacionadas con lineamientos cenozoicos de escala regional, fuertemente oblicuos respecto a la orientación del orógeno andino. Nosotros sugerimos que estos lineamientos son características heredadas al menos desde el Jurásico.

Palabras clave: Enjambre de diques, Emplazamiento de magma, Fábricas magnéticas, Transtensión, Transpresión, Jurásico, Estructuras NW-SE.

1. Introduction

Subduction zones concentrate crustal deformation caused by convergence of subducting and overriding plates. In these settings, deformation is more concentrated in the magmatic arc zone, where fluid circulation, the highest heat flow and consequently thermal weakening of the crust occur. Therefore, the analysis of magma emplacement mechanisms in ancient magmatic arc zones is a key tool to understand the tectonic behavior of the overriding plate during plate convergence. The Mesozoic arc of the central Andes exposed along the Coastal Ranges of north and central Chile has proved to be an exceptional site to describe and understand upper-plate deformation that occurred during Mesozoic subduction along the western margin of Gondwana. This exceptional situation reflects excellent bedrock exposures and the eastward migration of the magmatic arc from Triassic to Cretaceous time which has left older arc rocks comparatively intact.

Magmatic dikes, have been extensively used as paleostress indicators, based on the assumption that these structures are oriented normal to the least principal

stress (σ_3) during emplacement (e.g. Anderson, 1951). This simple model does not apply, however, if there are pre-existing fractures that can open following the σ_3 direction but are not oriented perpendicular to σ_3 . In these cases, dike orientation cannot be considered directly as paleostress indicators and a more careful analysis of emplacement mechanisms, mainly studying emplacement fabrics, is needed to understand how dikes are related to the stress state of the crust during magma intrusion (e.g., Delaney *et al.*, 1986; Blumenfeld and Bouchez, 1988; Féménias *et al.*, 2004; Clemente *et al.*, 2007). The study of emplacement mechanisms of dike swarms has been proved as can be an efficient tectonic tool to understand the evolution of ancient magmatic arcs (e.g. Glazner *et al.*, 1999).

This contribution seeks to describe and interpret Jurassic and Cretaceous dike swarms and associated Jurassic mafic plutonic rocks, exposed on the coastline of central Chile (33° and 33°45'S). To reach these goals, we combine field-based structural data, microstructural observations and AMS (anisotropy of magnetic susceptibility method) to get a detailed image of the internal fabric architecture of the dikes. This combination of methods is especially useful

in the case that dike fabric is not always evident or measurable in the field, as in the studied dike swarms. These results are discussed in terms of identification of the emplacement mechanisms of dike swarms and recognition of the regional deformation history (*e.g.*, transtension and transpression) during construction of the Jurassic to Cretaceous Coastal Batholith of central Chile.

2. Geological setting

Between the Late Permian and the Early Cretaceous, the Andean crust in north and central Chile was deformed as a retreating subduction boundary, characterized by mostly extensional and transtensional deformation (*e.g.*, Grocott *et al.*, 1994; Scheuber and González, 1999; Grocott and Taylor, 2002; Cembrano *et al.*, 2005). This deformation, mostly along the magmatic arc and the Atacama Fault Zone, was contemporaneous with the subsidence of Early Cretaceous basins in north and central Chile, in which large volumes of mantle-derived lavas accumulated (Vergara *et al.*, 1995; Aguirre *et al.*, 1999). Parada *et al.* (1999) proposed that progressive depletion in the Sr and Nd isotopic signature of magmas towards MORB from the Jurassic to the Cretaceous was caused by an increased amount of lithosphere removal and crustal thinning related to extension.

The Coastal Ranges between 33° and 33°45'S are mainly composed of Upper Paleozoic to Lower Cretaceous intrusive and volcanic rocks (Fig. 1a). In this segment, a well developed pattern of eastward-decreasing age is observed, from Lower Jurassic to Lower Cretaceous granitoid complexes and Mesozoic volcanic-sedimentary sequences (*e.g.*, Levi, 1973; Vergara *et al.*, 1995; Parada *et al.*, 1999). One striking feature of this area is the presence of NW-SE to WNW-ESE regional lineaments that crosscut the Coastal Ranges oblique to the current continental margin. These lineaments are in some cases related to large magnetic anomalies (*e.g.*, Yáñez *et al.*, 1998) and to Upper Paleozoic and Upper Jurassic belts of intrusive rocks (Fig. 1b).

2.1. Late Paleozoic-Triassic basement country rocks

The oldest units recognized in the area correspond to Upper Carboniferous granitoids (Hervé *et al.*, 1988; Gana *et al.*, 1996; Gana and Tosdal, 1996;

Wall *et al.*, 1996). These rocks range in composition from tonalite to granite (Siña, 1987; Arce, 2002). Granitoids crop out along the coastal line north of Valparaíso (33°S), between Quintay and El Tabo and at Santo Domingo (Fig. 1b). Seismic reflection data suggests that Upper Paleozoic granitoids continue to the west of the coastline of Valparaíso, forming an uplifted crustal competent block (Topocalma Knoll; Yáñez *et al.*, 2001). The age of the intrusions is constrained by U-Pb concordia ages and whole-rock Rb-Sr isochrons between 309 and 292 Ma (Godoy and Loske, 1988; Hervé *et al.*, 1988; Gana and Tosdal, 1996). The granitoids show foliation and lineation in most outcrops, defined by crystal and mafic enclave alignment. At a regional scale, the foliation in the granitoids varies in orientation between NW-SE to E-W with variable dips to the south, whereas mineral lineation plunges to the south. In addition to granitoids, tonalitic to granitic gneisses are distributed between Las Cruces and Cartagena, and at Quintay (Fig. 1b). These rocks display variable attitude of foliation and mineral and stretching lineations mostly plunging to the south, with local occurrence of high-strain ductile structures (shear zones and pencil lineations). The age of metamorphism is not totally clear. A dioritic gneiss from Cartagena yielded a zircon U-Pb age of 214±1 Ma (Gana and Tosdal, 1996), whereas at Quintay, the gneiss has ages of 290 Ma (zircon U-Pb concordia, Godoy and Loske, 1988). K-Ar age determinations in biotite, amphibole and plagioclase from the gneiss in Cartagena mostly gave Middle-Late Jurassic ages between 167 and 145 Ma (Cordani *et al.*, 1976; Hervé *et al.*, 1988; Gana *et al.*, 1996).

2.2. Jurassic-Early Cretaceous magmatic units

The volumetrically most important unit of the area corresponds to a NW-SE belt of Middle-Upper Jurassic granitoids that vary in composition between gabbro and granite (Gana *et al.*, 1996; Wall *et al.*, 1996). Some of these intrusive rocks show an intense ductile foliation, as observed in diorites from Laguna Verde area (Godoy and Loske, 1988). Precise titanite and zircon U-Pb radiometric dating define a pattern of decreasing ages to the east, from 163-160 Ma at Laguna Verde (Godoy and Loske, 1988) and 158±1 to 154±4 Ma eastern Limache and Sauce units, respectively, the two last located at 21 and 12 km east

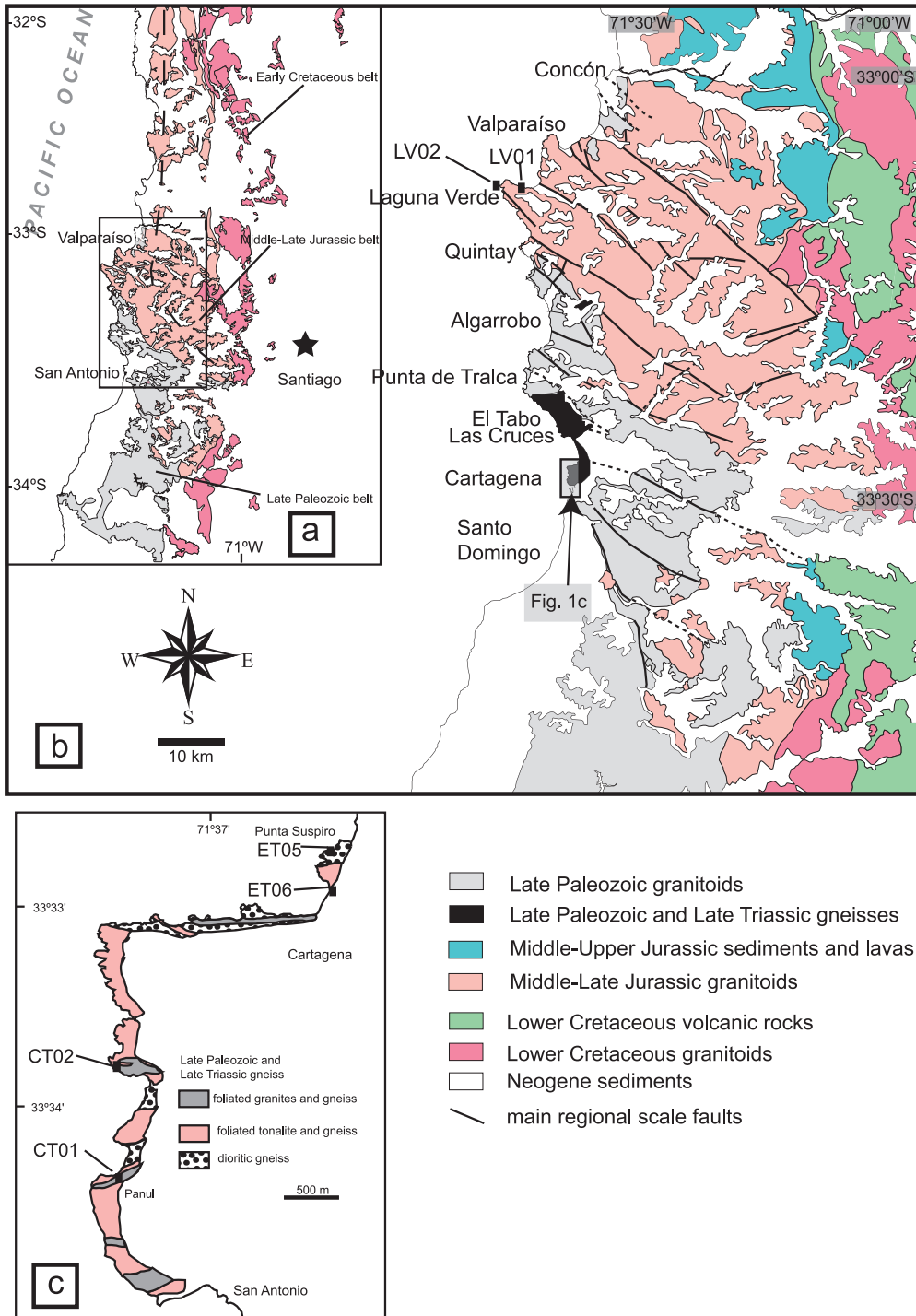


FIG. 1. **a.** Regional map showing the distribution of Late Paleozoic, Middle-Late Jurassic and Early Cretaceous batholithic belts. The segmented black line shows the approximate trend of the Jurassic batholith along the Coastal range. The solid square indicates the location of map of figure 1a; **b.** Geological map of the Coastal range of central Chile, between 33° and 33°45'S, modified from Gana *et al.* (1996), Wall *et al.* (1996) and SERNAGEOMIN (2002); **c.** Detail map of the Cartagena-San Antonio area, modified from Siña (1987), showing the location of AMS sampling sites.

of Laguna Verde (Gana and Tosdal, 1996). These ages are broadly similar to those obtained along the N-W belt exposed in the Coastal Ranges north of 33°S (Irwin *et al.*, 1987; Parada *et al.*, 1988). Lower-Upper Cretaceous granitoids occupy the eastern slope of the Coastal Ranges and vary in age between 118 and 91 Ma (Corvalán and Munizaga, 1972; Gana *et al.*, 1996; Parada *et al.*, 2005).

In addition to plutonic rocks, several mafic dike swarms have been recognized along the coastline between 33° and 33°45'S, mainly intruding the Upper Paleozoic basement. These are the Concon Mafic Dike Swarm (CMDS), Cartagena Mafic Dike Swarm (CrMDS) and El Tabo Dike Swarm (ETDS), which are described in detail below (section 4).

Between 33° and 33°45'S, Lower to Middle Jurassic volcanic and marine sequences (Ajial and Cerro Calera formations) are poorly exposed (Thomas, 1958; Piracés, 1976). Late Jurassic to Early Cretaceous successions are dominant in this segment of the Coastal ranges. They are characterized by large volume of mafic volcanic rocks. Upper Jurassic sedimentary rocks intercalated with volcanic sequences mark a change to subaerial deposition in the Late Jurassic (Vergara *et al.*, 1995).

3. Analytical methods

Microprobe analysis of mafic silicates (amphibole, pyroxene and biotite) and plagioclase of selected dike samples were carried out at the Geology Department of the Universidad de Chile, using a CAMECA SU-30 SEM-probe, with WDS, using a beam current of 10.15 nA, 15.11 kV of acceleration voltage and 5 to 20 µm beam size. Additional analyses were performed at ZELMI Laboratory, TU-Berlin, using a CAMEBAX microbeam electron microprobe, with PAP correction. Running conditions for these analyses were 13.1 nA beam current and 15.18 kV acceleration voltage. Accuracy is estimated as approximately 1% relative for major and 10% relative for minor elements.

⁴⁰Ar/³⁹Ar dating was carried out on hornblende separates from mafic dikes at the Geochronology Laboratory of Servicio Nacional de Geología y Minería (SERNAGEOMIN). Approximately one kilogram of sample was crushed and sieved to obtain grain sizes of 100 to 250 µm. Amphibole and biotite were separated using an isodynamic magnetic separator and heavy liquids, followed by hand picking

under a binocular microscope. The samples were irradiated in the nuclear reactor of the Comisión Chilena de Energía Nuclear (La Reina, Santiago de Chile). The irradiation factor for each sample was $J=0.0010241\pm 7.9\times 10^{-6}$ (sample CC-03-66) and $J=0.0010502\pm 8.1\times 10^{-6}$ (sample CC-03-27). Gas extraction was performed using a step heating procedure with a CO₂ laser beam on hornblende grain populations (<15 grains). Detailed analytical procedures are given in Arancibia *et al.* (2006). The criteria used to define a plateau age are that it should contain more than 50% released ³⁹Ar, that there should be at least three successive steps in the plateau, and that the integrated age of the plateau should agree with each apparent age of the plateau within 2σ.

Sampling for AMS was carried out using an oil-powered drill at 4 sites (34 samples) of the CrMDS and 2 sites (24 samples) of Laguna Verde diorites. Sampling in dikes was carried out especially along dike margins but also in central part of dikes, for a better characterization of internal fabric. Samples were oriented using solar and magnetic compasses. The anisotropy of magnetic susceptibility (AMS) of the samples was measured and thermomagnetic experiments were conducted at the Laboratorio de Paleomagnetismo, Departamento de Geología, Universidad de Chile, using KLY-3S Kappabridge equipment (AGICO Ltd.), working under a weak alternative magnetic field, with a resolution as high as 10⁻⁸ SI. IRM (isothermal remanent magnetization) experiments at the same laboratory were performed using an ASC IM-10-30 Impulse Magnetometer.

4. Mesozoic dike swarms and Laguna Verde diorites

Mafic dike swarms, recognized along the coastline of central Chile (Muñoz-Cristi, 1964; Irwin *et al.*, 1987; Creixell *et al.*, 2006), will be described in terms of petrography and structures. In addition, the main structural and petrographic features of plutonic rocks located at Laguna Verde will be also described, because these intrusions are coeval and spatially associated with Jurassic dike swarms.

4.1. Concón Mafic Dike Swarm (CMDS)

This dike swarm is recognized along the coastal road between Concón and Viña del Mar and intruded into foliated Late Paleozoic granitoids. This dike

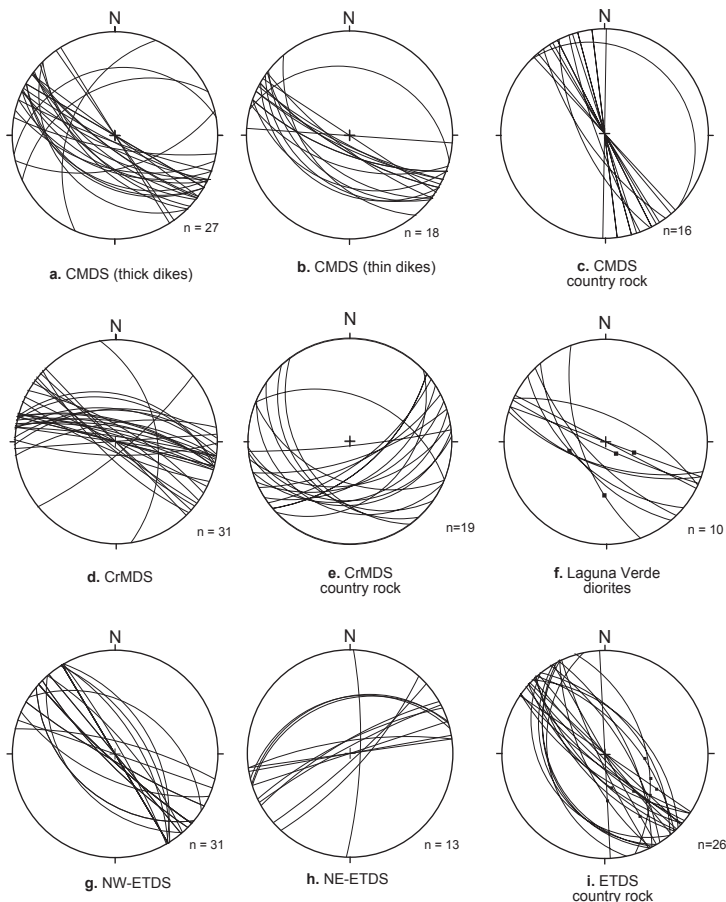


FIG. 2. Stereonet diagrams for orientation of mafic dikes of the **a.** CMDS (thick dikes), **b.** CMDS (thin dikes), **c.** CMDS country rocks (foliated granitoids), **d.** CrMDS **e.** CrMDS country rocks (gneiss and amphibolites), **f.** Laguna Verde diorites, **g.** ETDS, NW-striking dikes, **h.** ETDS, NE-striking dikes, and **i.** ETDS country rocks (foliated granitoids).

swarm, described in detail by Creixell *et al.* (2006), consists of two generation of basaltic-andesitic dikes, an early group of thick dikes (mostly between 5 and 12 m thickness), intruded by thin dikes (0.5-3 m thickness). All of these dikes strike NW-SE (Figs. 2a and 2b). The thick dikes are characterized by the presence of pervasive ductile deformation at thin section scale (Fig. 3a and 3b), whereas thin dikes show a magmatic foliation. Two amphibole $^{40}\text{Ar}/^{39}\text{Ar}$ ages of 157 and 163 Ma on deformed (thick) and undeformed (thin) dikes, respectively, broadly indicate that emplacement of the dike swarm occurred in the Middle-late Jurassic (Creixell *et al.*, 2006).

4.2. Cartagena Mafic Dike Swarm (CrMDS)

This swarm consists of basaltic dikes that are 1.5 m thick and crop out between Santo Domingo and Cartagena (Fig. 1c). Some of the dikes locally reach 2 to 2.5 m thickness. The strike of the dikes varies between NW-SE and E-W with a mean orientation of $287^\circ/80^\circ\text{N}$ (Fig. 2d). NE-striking dikes were locally observed at Panul, but their crosscutting relations with the other dikes were not observed. The density of dikes is largely variable, reaching maximum densities of approximately 20 to 30% of the outcrop in local sections (profiles 300 to 500 m in length) in Cartagena beach. The country rocks include Upper Triassic dioritic gneiss, mylonitic gneiss and Upper Paleozoic granitoids with variable fabric orientation (Fig. 2e).

These dikes are composed of an equigranular to porphyritic arrangement of intergranular amphibole (Mg-hornblende to tschermakite), plagioclase (An_{30-62}), biotite, low-Ti magnetite and accessory pyrrhotite, pyrite and apatite, with amphibole (mostly Mg-hornblende) and plagioclase (An_{59-82}) phenocrysts. Pyrrhotite occurs as inclusions in amphibole, in the same way as in late thin dikes of CMDS (Creixell *et al.*, 2006). Phenocrysts mostly correspond to Mg-hornblende. Some strongly altered dikes of this swarm are characterized by a planar fabric, but extreme replacement of hornblende by chlorite prohibits to recognize the magmatic texture.

The age of the dike swarm is only constrained by a new hornblende $^{40}\text{Ar}/^{39}\text{Ar}$ plateau age of 157 ± 3 Ma (Fig. 4a, 4b. Details of the analysis are given in table 1 of supplementary data). Late Jurassic K-Ar

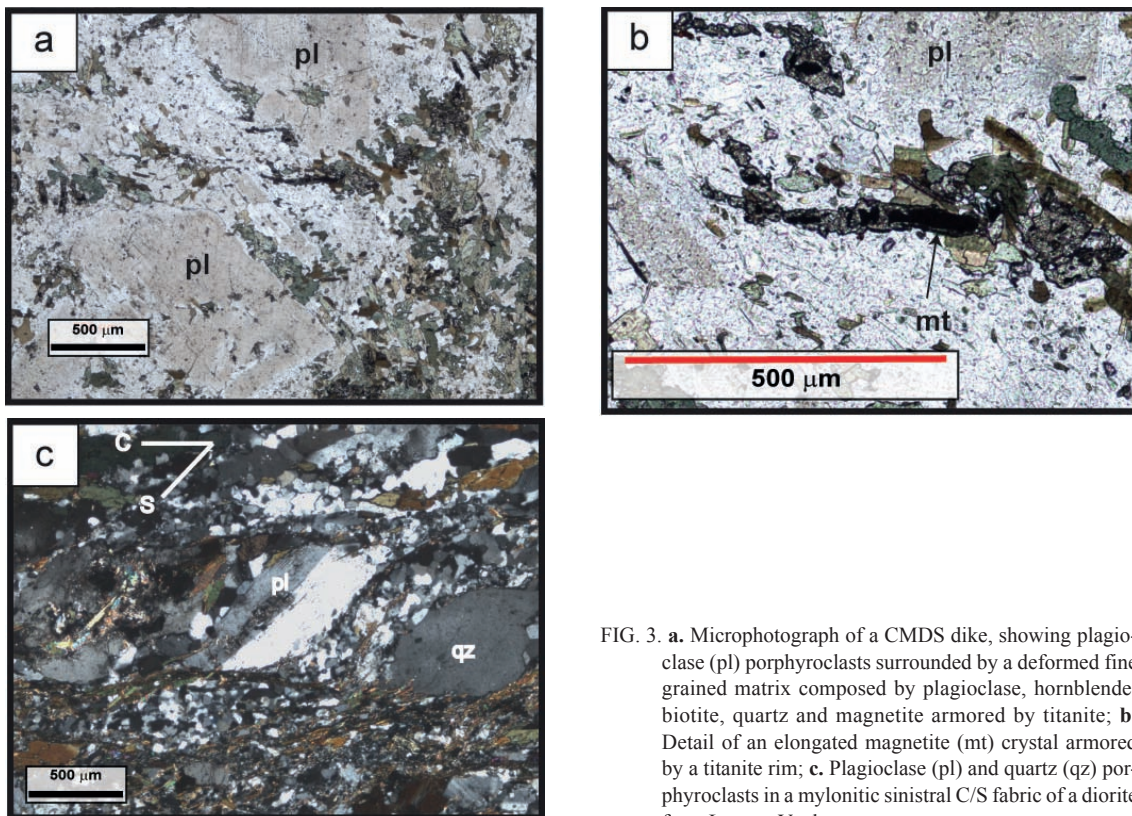


FIG. 3. **a.** Microphotograph of a CMDS dike, showing plagioclase (pl) porphyroclasts surrounded by a deformed fine grained matrix composed by plagioclase, hornblende, biotite, quartz and magnetite armored by titanite; **b.** Detail of an elongated magnetite (mt) crystal armored by a titanite rim; **c.** Plagioclase (pl) and quartz (qz) porphyroclasts in a mylonitic sinistral C/S fabric of a diorite from Laguna Verde.

ages obtained by Gana *et al.* (1996) in Upper Triassic gneissic host rocks from Cartagena are interpreted to reflect extensive thermal resetting by the intrusion of the CrMDS.

4.3. Laguna Verde diorites

This unit consists of gabbroic to dioritic intrusive rocks and some gneissic diorites, with minor felsic components (Hervé, 1976; Godoy and Loske, 1988). Deformation on this unit is largely variable in space, but diorites with intense ductile deformation (gneissic diorites) tend to coincide with location of most prominent NW-SE lineaments in the area. The age of relatively undeformed diorites (two-pyroxene diorite) is constrained by zircon U-Pb concordant ages between 163-160 Ma (Godoy and Loske, 1988). Zircons from gneissic diorites in this unit show similar concordant ages of 163 Ma (Godoy and Loske, 1988). According to these authors, slight dispersion in the ages is probably related to variable amount of Pb loss in the zircons. An $^{40}\text{Ar}/^{39}\text{Ar}$ age of 165 ± 2.6

Ma in hornblende from diorites (Irwin *et al.*, 1987) partially overlaps with these U-Pb ages. A younger Rb-Sr mineral isochron age of 156.3 ± 1.2 Ma (Godoy and Loske, 1988) show variable degree of isotopic disequilibrium and could be affected by post-crystallization alteration processes.

Laguna Verde diorites show coarse-grained texture. Deformed diorites are formed by sigmoidal plagioclase (An_{48-52}) and amphibole (mostly Fe-Mg hornblende and minor Fe-edinite) porphyroclasts, in a matrix of statically recrystallized hornblende, plagioclase (An_{25-36}), quartz, titanite, magnetite and accessory allanite (armored by epidote). In some samples, S/C microstructures are well developed between matrix and porphyroclasts (Fig. 3c).

4.4. Structures in Jurassic dikes and Laguna Verde diorites

The different types of planar structures (dike margins, foliations and shear zones) recognized in Jurassic dikes and diorites strike dominantly to the

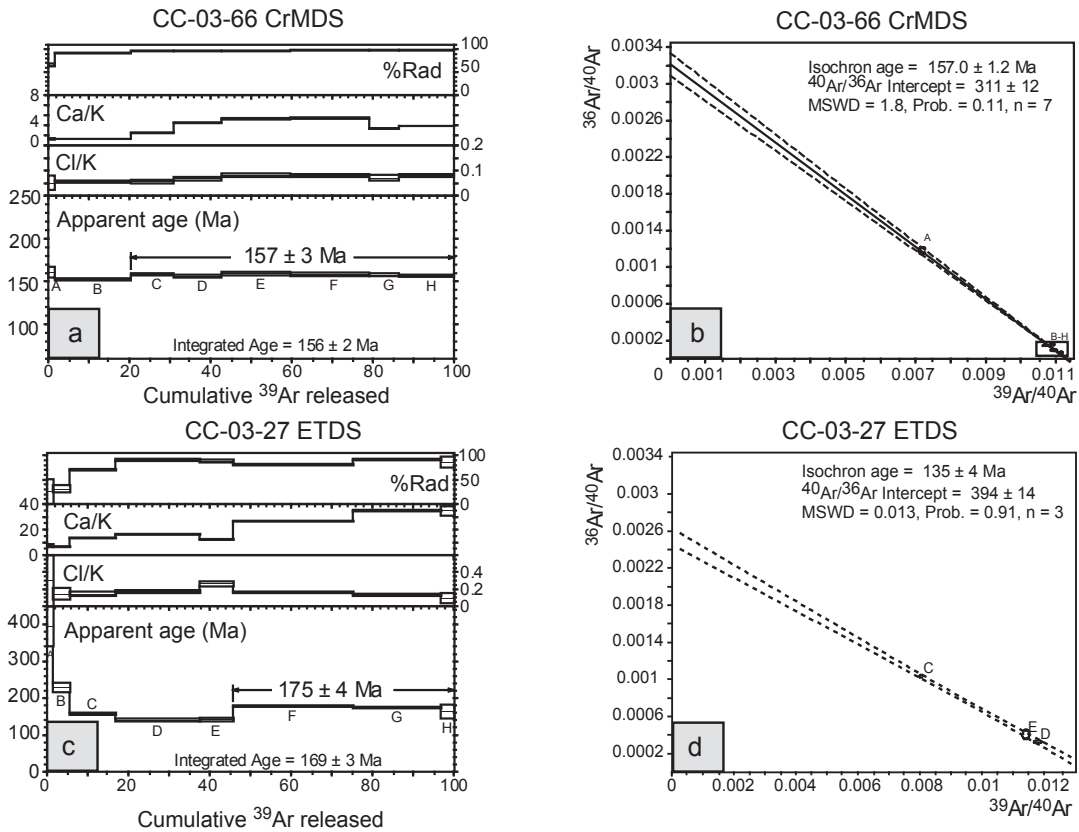


FIG. 4. **a.** $^{40}\text{Ar}/^{39}\text{Ar}$ age spectra for sample CC-03-66 (CrMDS); **b.** Inverse isochron; **c.** $^{40}\text{Ar}/^{39}\text{Ar}$ age spectra for a mafic dike of the ETDS; **d.** Inverse isochron.

NW-SE. In the CMDS, thick and thin dikes show internal foliations that are clockwise oblique to dike margins. Passive markers with sinistral offsets at each side of the dikes are locally observed. In vertical sections, thin dikes show a trace of steep lineations and sigmoidal xenoliths indicating reverse shearing along dike walls. Some thin dikes are near horizontal. Variations from solid-state to magmatic microfabrics in thick dikes and magmatic fabrics in thin dikes suggest that the whole swarm can be considered as syntectonic (Creixell *et al.*, 2006). In CrMDS at Cartagena, a set of the near-vertical dikes resemble the thin dikes of CMDS and are ductilely deformed where are cut by nearly coeval E-W reverse faults (Figs. 5a, b). Horizontal dikes of the CrMDS are observed in the Santo Domingo area (Figs. 5c, d). In most cases, we can note that the orientations of the mafic dikes differ from the orientation of the host rock fabric (Figs. 2a to 2e).

Structures of Laguna Verde diorites were mainly studied at two localities, especially where the NW-SE shear zones terminate westwards at the surface. In the northern locality studied, near-vertical sinistral shear foliation is spatially associated with meter-scale sub-vertical folds and ductile reverse shear zones. Shear foliation is oriented 110° - $160^\circ/65^\circ$ - 90° SW and stretching lineations plunge to the south (46° - 77° , Fig. 2f). The microfabrics in these deformed diorites show sinistral C/S fabrics, with evidence of high-temperature ductile deformation on δ -type porphyroclasts (sigmoidal shape in plagioclase and amphibole) and foliated and recrystallized matrix.

4.5. El Tabo Mafic Dike Swarm (ETDS)

This swarm consists of two systems of dikes of basaltic composition that mainly occur between Algarrobo and El Tabo. Such dikes are sparse at

TABLE 1. DETAILED $^{40}\text{Ar}/^{39}\text{Ar}$ RESULTS ON BIOTITE AND AMPHIBOLE FROM MAFIC DIKES, COASTAL RANGE, CENTRAL CHILE.

amphibole sample CC-03-66							
CrMDS							
Step	Atmospheric contamination	^{39}Ar (%)	$^{40}\text{Ar}/^{36}\text{Ar}$	$^{40}\text{Ar}/^{39}\text{Ar}$	Ca/K	$^{40*}\text{Ar}/^{39}\text{Ar}$	Age
3-A	0.1	1.7	846.024	139.470	1.17503	90.8079	160.799±3.12
8-B	0.7	18.7	3,146.633	94.607	1.18832	85.72222	152.162±0.55
10-C	3	10.6	6,944.444	93.023	2.39927	89.07796	157.866±0.65
12-D	5	11.8	6,414.368	91.996	4.44332	87.75354	155.617±0.86
13-E	6.2	17.1	6,915.629	93.545	5.23301	89.55682	158.678±0.95
14-F	9.5	19.4	10,515.247	91.575	5.37026	88.97907	157.698±1.04
18-G	6	7.2	10,395.010	91.575	3.3095	88.9904	157.717±0.79
30-H	9.9	13.5	15,313.936	89.847	3.77822	88.10347	156.211±0.68
Integrated Age=							156±2
Plateau Age =		79.6%					157±3
amphibole sample CC-03-27							
ETDS							
Step	Atmospheric contamination	^{39}Ar (%)	$^{40}\text{Ar}/^{36}\text{Ar}$	$^{40}\text{Ar}/^{39}\text{Ar}$	Ca/K	$^{40*}\text{Ar}/^{39}\text{Ar}$	Age
3-A	0	1.6	341.986	1694.915	6.965	231.975	394.272±27.47
8-B	0.1	4	428.137	413.223	6.238	128.226	228.462±6.30
10-C	1.7	11.2	966.744	124.688	13.181	86.578	157.374±1.59
12-D	9.1	20.8	3,074.085	84.818	16.079	76.680	140.061±1.68
13-E	5.5	8.3	2,463.054	87.719	12.261	77.227	141.021±2.62
16-F	5.3	29.5	1,497.903	121.803	26.306	97.831	176.858±0.97
20-G	15.5	21.6	3,259.452	105.597	34.560	96.040	173.771±1.00
30-H	10.1	3.1	2,008.435	104.822	34.047	89.394	162.269±9.47
Integrated Age=							169±3
Plateau Age =		54.2%					175±4

Cartagena and Las Cruces. The dikes intrude foliated Late Paleozoic granitoids. One system of intrusions comprises porphyritic to aphanitic NW-striking dikes, with a mean thickness of 0.6 m and mean orientation of 137°/89°W (Fig. 2g), usually occurring as a group of multiple parallel intrusions. Its texture comprises subparallel plagioclase phenocrysts (An_{53-74}) and amphibole prisms (mostly tschermakite and minor proportion of Mg-hastingsite) and clinopyroxene ($\text{Wo}_{28}\text{En}_{48-50}\text{Fs}_{20-23}$) phenocrysts, with abundant brown hornblende prisms in the groundmass, accompanied by accessory titanite, magnetite and locally chromite. The other system comprises NE-striking dikes (main orientation: 65°/79°N, Fig. 2h) of variable thickness between 0.5 and 4 m (mean thickness of 2.6 m). The rocks are porphyritic and contain plagioclase phenocrysts

in a medium-grained groundmass of clinopyroxene ($\text{Wo}_{40-42}\text{En}_{29-31}\text{Fs}_{26-29}$) and plagioclase (An_{52-53}) accompanied by ilmenite, apatite and minor biotite. A relevant field observation is that both dike systems show mutual crosscutting relations between them.

The age of the dike swarm is poorly known. An imprecise new hornblende $^{40}\text{Ar}/^{39}\text{Ar}$ age from a NW-SE dike yields a plateau age of 175±4 Ma involving 54.2% of ^{39}Ar released (Fig. 4c, details of the analyses are given in table 1 of supplementary data), but incremental release pattern show a typical 'U-shaped' shape, with relatively high apparent ages in the first two incremental heating steps, a relatively flat pattern in the C, D and E steps and finally again higher apparent ages in steps F to G. This kind of degasification pattern is indicative of

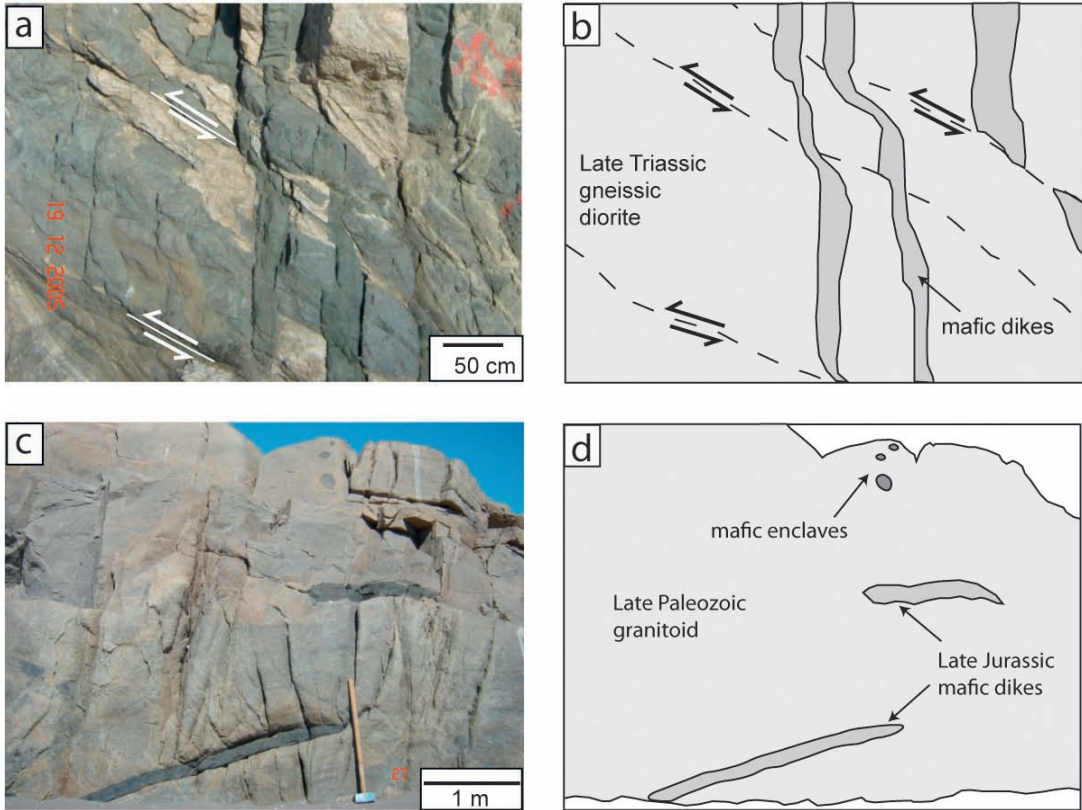


FIG. 5. Field features of CrMDS and Laguna Verde diorites, with schematic representation of the outcrops at the right side of the photograph (b, d); a. Mafic dikes of the CrMDS displaced and ductilely sheared by reverse faults. Away from the dike, the faults evidence fragile deformation. View to the east, c. Near-horizontal CrMDS dike intruding Late Paleozoic granitoids at Santo Domingo beach, view to the south.

Ar excess in the sample. According to this, the lower apparent ages contained in steps D and E (140.1 and 141.0 Ma) could represent the maximum ages for the sample. These two steps are characterized by lower Ca/K ratios with respect to high temperature steps, pointing to important heterogeneities in the sample and possible degasification of calcic phases at high temperature (plagioclase inclusions). The influence of Ar excess in the analyses is favored by the very low K_2O of the analyzed amphiboles (between 0.098 and 0.223 wt%). This possible Early Cretaceous age is similar to K-Ar and $^{40}Ar/^{39}Ar$ ages between 144.4 and 151 Ma determined in dike swarms north of the study area near $32^{\circ}30'S$ (Irwin *et al.*, 1987); and also in Lower Cretaceous bimodal dike suites (138 ± 1 Ma) south of the study area (Willner *et al.*, 2005).

4.6. Structures in the Cretaceous ETDS

Unlike the Jurassic intrusions, the ETDS dikes do not show evidences of ductile deformation. Some outcrops contain dike-parallel joints in country rocks close to the dikes (Figs. 6a a, b). Some chlorite-epidote veins cross-cut by NW-striking dikes indicate dike opening normal to the walls (Figs. 6c, d, e, f). NW-striking dikes form sets of multiple sub-parallel intrusions. At Punta de Tralca, dikes are more abundant and more closely spaced. The spacing between dikes in this locality is very low (0 to 0.3 m) and the abundance of dikes locally reach about 20% of the outcrop area. To the north and south, the abundance of dikes diminishes drastically (<2% of the outcrop at El Tabo) and spacing between dikes increase in the order of 2 to 10 m.

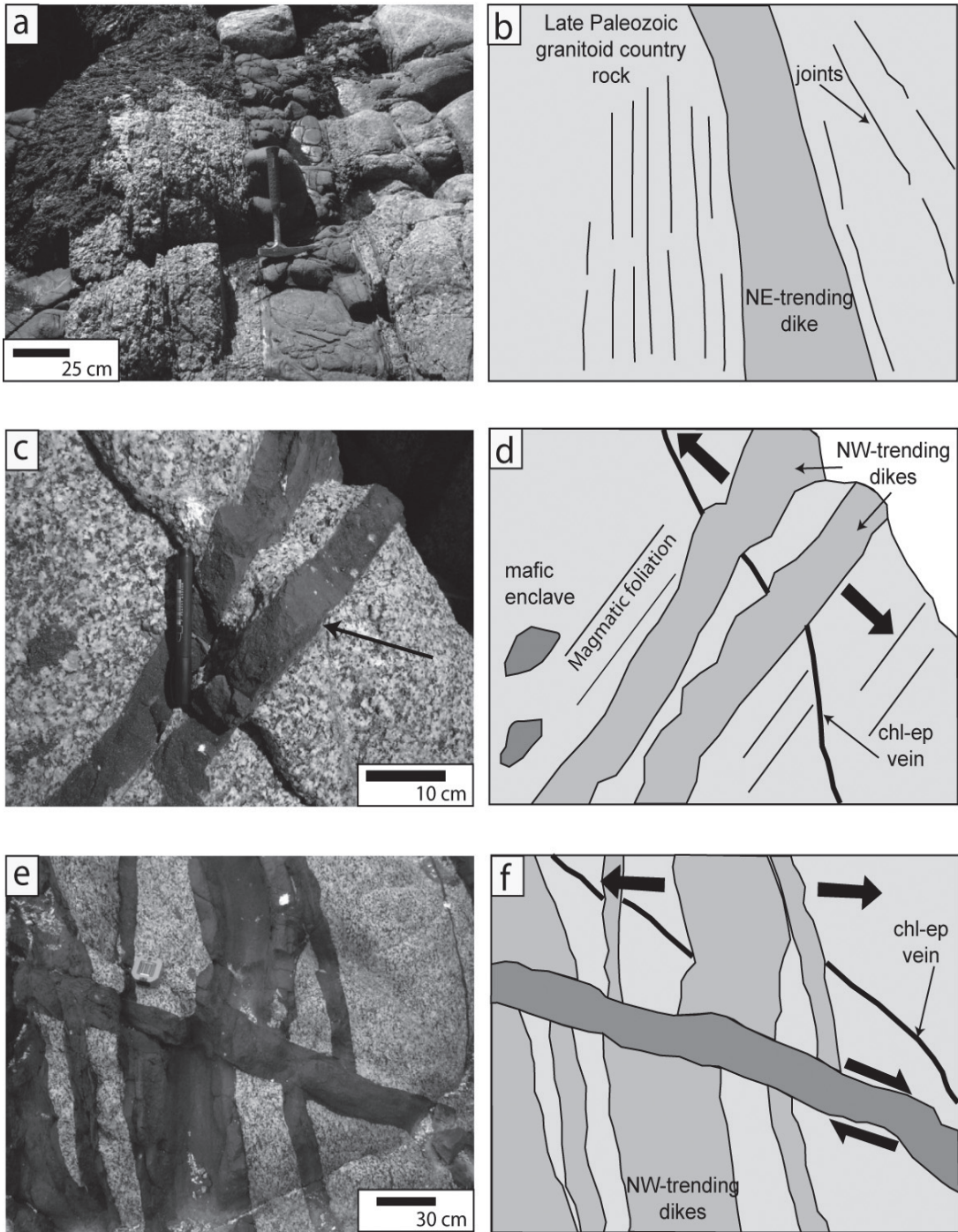


FIG. 6. Field features of the ETDS, with schematic representation of the outcrops at the right side of the photograph (Figs. b, d, f) **a.** NE-striking dike of the ETDS with associated dike-parallel joints in the granitoid country rocks, El Quisco beach, view to the NE, hammer for scale; **c.** NW-striking mafic dike of ETDS cut chlorite-epidote vein (chl-ep). This vein is displaced normal to dike walls. Punta de Tralca beach, horizontal section, pen for scale; **e.** near-vertical, zoned NW-striking mafic dike intruding chlorite-epidote vein, displaced normal to dike walls in vertical section. This section is cut and normally displaced by another, gently-dipping, NW-striking dike. Punta de Tralca beach, magnetic compass for scale.

The orientations of both NW- and NE-striking dike sets are homogeneous and do not show similarities with orientation of the country rock foliation measured in El Tabo, Punta de Tralca and Las Cruces (Fig. 2g to 2i).

5. AMS fabrics of dike swarms and Laguna Verde diorites

The AMS (anisotropy of magnetic susceptibility) represents the directional variability of the magnetic susceptibility of a sample (*e.g.*, Tarling and Hrouda, 1993). This is represented by a second-order tensor with a magnetic ellipsoid defined by three eigenvectors ($K_1 > K_2 > K_3$), where K_1 represents the magnetic lineation and K_3 represents the pole of the magnetic foliation plane (K_1 - K_2 plane). The mean magnetic susceptibility K_m corresponds to the arithmetic mean of the magnitude of three vectors ($K_m = [K_1 + K_2 + K_3]/3$). The degree of anisotropy of the magnetic ellipsoid (%P') corresponds to the P_j defined by Jelinek (1981). The shape parameter T for the magnetic ellipsoid indicates oblate shapes when $0 \leq T \leq 1$ and prolate shapes when $-1 \leq T \leq 0$.

In most igneous rocks, the magnetic susceptibility is related to the presence of ferromagnetic minerals and to a lesser degree to the presence of paramagnetic phases. The source of the AMS could come from 'crystalline anisotropy' (variations in magnetization controlled by the distribution of cations in the crystal structure), 'distribution anisotropy', derived from magnetic interaction among magnetic grains (when they tend to form clusters of grains) and shape anisotropy, defined by the variation of susceptibility in nonequidimensional grains, where K_1 tends to be parallel to the long axis of the particle. In the last case the AMS ellipsoid tends to show a good correspondence with the shape fabric ellipsoid, because the individual ferromagnetic grains (*e.g.*, magnetite) tend to be late phases in the crystallization sequence of igneous rocks and occupy the space between the rock-forming minerals.

5.1. Magnetic properties and AMS ellipsoids

The magnetic properties and AMS directions of the CMDS and ETDS were described in detail by Creixell *et al.* (2006, 2009, respectively). Details of the new analyses are given in table 2 of supplementary data.

Examination of selected samples of CrMDS under SEM (scanning electron microscopy) and EMPA (electron microprobe analyses) allows us to detect the presence of low-Ti magnetite as independent crystals in the oriented groundmass of dikes and small inclusions of pyrrhotite in primary hornblende, in a similar way as observed in thin dikes of CMDS. The presence of magnetite is confirmed by IRM experiments in which magnetic saturation was reached at approximately 250 mT (Fig. 7a). The presence of low-Ti magnetite is also suggested by demagnetization experiments and Curie temperatures near 570°C (Fig. 7b). In these experiments, demagnetization close to 320°C in some samples of CrMDS indicate the presence of monoclinic or mixed monoclinic-hexagonal pyrrhotite (*e.g.*, Martín-Hernández *et al.*, 2008) which agrees with petrographic observations.

Samples of the four sites of CrMDS show weak ferromagnetic behavior, with K_m between 824 and 394×10^{-6} [SI] (Fig. 7c). CrMDS dikes have low but variable %P' (0.7-3.5%) at relatively constant K_m values, suggesting that intensity of magnetic fabric is not controlled by composition, *e.g.* magnetite content (Fig. 7c). %P' tends to be higher in sites ET05 and ET06 from Punta Suspiro. This is well correlated with field observations of incipient internal shape foliation in these dikes, which was not clearly observed in sites at Panul. The shape parameter T varies independently of K_m values in dikes in the Panul area. In both sites at Punta Suspiro, most ellipsoids are oblate, with variations not correlated with variations in K_m (Fig. 7d). This also suggests, as for the anisotropy degree, that the shape of the magnetic ellipsoids (T) is not controlled by magnetic susceptibility (*e.g.*, magnetite or pyrrhotite content). Indeed, the shape parameter T tends to be correlated with anisotropy degree %P', especially in sites ET05 and ET06 of Punta Suspiro, where %P' is higher (Fig. 7e, f).

Significant differences were found between the AMS ellipsoids of ETDS and CMDS samples. K_m and %P' are strongly correlated in thick CMDS dikes (Fig. 7c). In these dikes, higher %P' tends to correspond to triaxial to prolate ellipsoids (Fig. 7e). These relations indicate that higher susceptibility rocks are also more anisotropic. The magnetic ellipsoids of thin dikes of CMDS tend to be similar to those of the CrMDS, because we can observe a tendency to positive correlation between %P' and

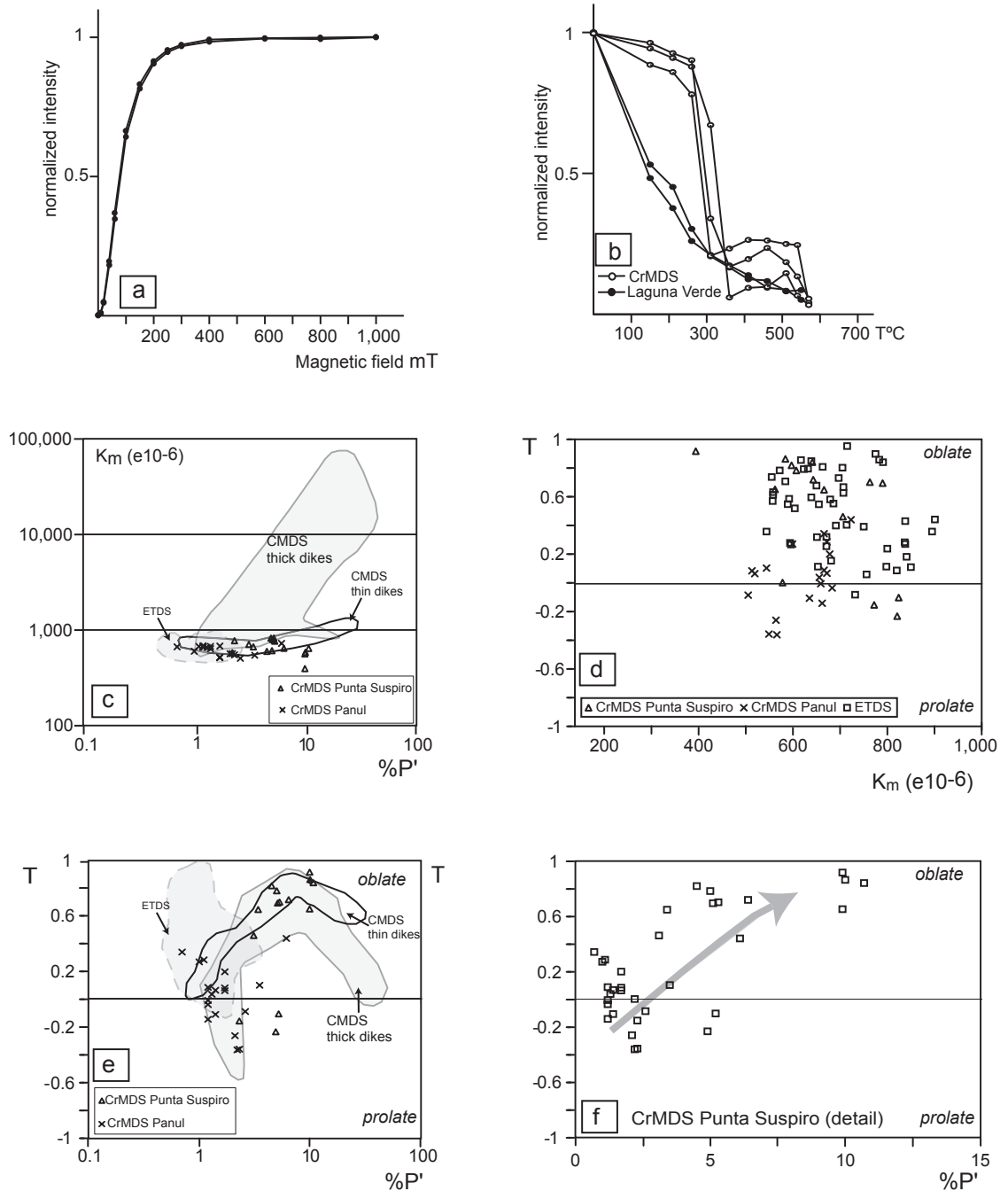


FIG. 7. **a.** IRM curves for CrMDS samples; **b.** Demagnetization experiments in CrMDS samples, showing two marked demagnetization temperatures near 320°C and 570°C, suggesting the presence of pyrrhotite and low-Ti magnetite in the samples; **c.** Bulk magnetic susceptibility (Km) versus magnetic anisotropy degree (%P') in samples from CrMDS. Samples from ETDS and CMDS are shown for comparison; **d.** Shape parameter (T) versus bulk magnetic susceptibility in samples from CrMDS; **e.** Shape parameter (T) versus magnetic anisotropy degree (%P') in samples from CrMDS. Samples from ETDS and CMDS are shown for comparison; **f.** Detail from **e.** for samples of CrMDS from Punta Suspiro locality (sites ET05 and ET06), showing the correlation between T and %P' in these samples (grey arrow).

TABLE 2. AMS DATA FOR THE CrMDS AND LAGUNA VERDE DIORITES.

	Km					K1		K2		K3	
	(10 ⁻⁶ SI)	P'	T	L	F	dec	inc	dec	inc	dec	inc
04LV0101a	695.5	8.2	0.438	1.022	1.057	88	33	306	51	191	19
04LV0101b	747.7	8.8	0.507	1.02	1.063	85	36	303	47	190	20
04LV0102b	652.7	8.7	0.402	1.025	1.059	98	71	320	14	227	12
04LV0103a	619.3	8.5	0.322	1.028	1.054	144	69	305	20	37	6
04LV0104a	881.4	12.2	0.369	1.036	1.08	170	77	320	11	51	6
04LV0104b	782.4	8.4	0.167	1.034	1.048	148	55	307	34	44	10
04LV0105a	906.5	10.4	0.022	1.049	1.052	134	28	306	61	43	3
04LV0105b	1,374	34.1	0.089	1.143	1.173	112	57	308	32	214	7
04LV0106a	742.5	16.7	0.068	1.074	1.086	122	55	295	34	27	3
04LV0201a	12,480	25.5	-0.236	1.149	1.09	195	36	299	17	49	48
04LV0202a	16,520	40	-0.218	1.225	1.139	186	36	304	33	62	36
04LV0202b	14,620	36.6	-0.107	1.188	1.149	187	35	301	30	60	40
04LV0203a	4,490	15.3	-0.512	1.109	1.034	212	13	318	50	111	37
04LV0203b	9,327	20.9	-0.306	1.13	1.067	212	14	313	39	106	48
04LV0204a	8,597	51.1	-0.164	1.27	1.187	211	46	346	35	94	24
04LV0205a	30,100	63	0.17	1.224	1.329	236	28	329	5	68	61
04LV0205b	29,190	58.1	0.154	1.213	1.301	234	27	326	4	64	62
04LV0206a	81,960	48.1	0.236	1.16	1.272	235	36	330	7	69	54
04LV0206b	79,340	50.9	0.255	1.164	1.291	235	37	329	6	68	53
04LV0207a	51,930	48.6	-0.327	1.295	1.14	232	39	342	23	95	42
04LV0207b	73,040	46.8	-0.069	1.228	1.196	231	38	341	24	95	42
04LV0209a	43,220	84.7	0.558	1.138	1.572	196	64	332	19	67	17
04LV0209b	18,150	77.5	0.523	1.14	1.519	190	63	331	22	67	15
04LV0210a	52,830	27.8	-0.008	1.131	1.129	219	45	4	39	110	18
05CT0101a	566	1.023	-0.362	1.015	1.007	14.5	-42.1	338.1	41.7	86.2	19.2
05CT0101b	564	1.021	-0.26	1.013	1.008	10.1	-42.6	335.7	41.9	82.7	18.0
05CT0102a	549	1.023	-0.357	1.015	1.007	12.2	-39.6	342.9	46.5	89.4	15.0
05CT0103a	505	1.026	-0.086	1.014	1.012	3.2	-50.7	335.0	35.8	75.4	14.0
05CT0104a	519	1.017	0.064	1.008	1.009	350.2	-34.5	328.0	53.4	72.7	10.7
05CT0104b	513	1.017	0.084	1.008	1.009	351.3	-39.0	334.0	49.7	74.3	8.6
05CT0105a	544	1.035	0.103	1.015	1.019	347.8	-29.4	319.8	57.4	70.5	12.7
05CT0106a	723	1.063	0.44	1.017	1.043	217.0	73.0	78.2	13.0	345.7	10.8
05CT0201a	662	1.012	-0.142	1.007	1.005	51.5	-44.6	219.8	-44.8	315.7	-5.9
05CT0202a	683	1.012	-0.036	1.006	1.006	46.7	-47.5	225.2	-42.5	315.9	-0.8
05CT0203a	635	1.014	-0.107	1.008	1.006	56.8	-37.3	219.6	-51.4	320.3	-8.4
05CT0204a	672	1.012	0.286	1.004	1.007	58.6	-42.6	207.6	-43.0	313.2	-16.1
05CT0205a	659	1.012	-0.006	1.006	1.006	59.8	-38.9	202.7	-44.6	313.2	-19.5
05CT0206a	678	1.017	0.2	1.007	1.01	53.8	-27.9	205.2	-58.9	317.0	-12.6
05CT0207a	672	1.014	0.067	1.006	1.007	61.7	-33.4	214.2	-53.4	322.7	-13.3
05CT0208a	666	1.007	0.342	1.002	1.005	57.6	-30.4	192.3	-50.2	313.1	-23.1
05CT0209a	599	1.01	0.271	1.004	1.006	48.4	-29.3	213.7	-59.9	314.8	-6.4
05CT0210a	656	1.013	0.038	1.006	1.007	54.5	-36.2	210.7	-51.4	315.8	-11.7
05CT0210b	666	1.012	0.088	1.006	1.007	53.2	-40.3	214.7	-48.1	315.2	-9.3

Table 2 continued.

	Km					K1		K2		K3	
	(10 ⁻⁶ SI)	P'	T	L	F	dec	inc	dec	inc	dec	inc
04ET0504a	562	1.099	0.652	1.016	1.076	303.8	63	60.1	-15.6	163.3	21.4
04ET0505a	641	1.107	0.841	1.007	1.076	305.8	60.1	223.6	-4.5	136.2	29.5
04ET0506a	597	1.045	0.819	1.004	1.037	29.1	24.2	253.1	58	128.4	19.6
04ET0506b	607	1.05	0.783	1.005	1.041	37.6	11.9	277.3	67.2	131.7	19.1
04ET0509a	643	1.064	0.719	1.008	1.05	127	72.2	51.9	-4.7	323.3	17.1
04ET0511a	394	1.1	0.864	1.006	1.083	85.3	-1.8	187	-81.1	355.1	-8.8
04ET0511b	394	1.099	0.917	1.003	1.083	85.6	17.8	105.4	-71.1	357.6	-6
04ET0601a	824	1.052	-0.103	1.029	1.023	11.5	77.1	86.3	-3.4	355.5	-12.4
04ET0602a	821	1.049	-0.232	1.03	1.018	12.6	77.3	58.8	-8.9	327.4	-9.1
04ET0603a	578	1.022	0.002	1.011	1.011	64	72.1	60.7	-17.9	331	1
04ET0603b	772	1.023	-0.154	1.013	1.01	50.1	53.6	52.2	-36.4	321.5	-1
04ET0604a	666	1.034	0.648	1.005	1.026	57.4	52.9	112.4	-23.5	9.7	-26.9
04ET0604b	706	1.031	0.461	1.008	1.022	68.1	62.2	117.4	-19	20.4	-19.5
04ET0605a	763	1.053	0.702	1.007	1.042	63.5	42.5	104.8	-39.4	355.3	-22.1
04ET0605b	790	1.051	0.695	1.007	1.04	74.9	22.6	119.1	-59.8	353.1	-18.9

T (Fig. 7e) and variations of %P' independently of K_m values (Fig. 7c). Magnetic properties of ETDS are distinguishable from CMDS and CrMDS. ETDS samples are characterized by low K_m between 544 to 841×10^{-6} [SI] in NW-striking dikes and 651 to 901×10^{-6} [SI] in NE-striking dikes, whereas most AMS ellipsoids are dominantly oblate with low %P' (close to 1%). The weak ferrimagnetic behavior of these dikes has not been studied in terms of contributions of magnetite and paramagnetic minerals in the source of magnetic susceptibility.

5.1.1. Directional data

In sites ET05 and ET06 from Punta Suspiro, the magnetic foliation is near parallel to the dike walls and magnetic lineation plunges steeply to the NE (Fig. 8). The fact that these dikes are cut by reverse shear zones will be discussed below in terms of the origin of these fabrics. In site CT01 from Panul, magnetic lineation gently plunges to the SW, whereas the magnetic foliation poles are well-clustered, with foliation planes (K_1 - K_2 planes) striking NNW-SSE, clockwise oblique to the dike trend (Fig. 8), in a pattern similar to that observed in the magnetic and shape fabrics of the CMDS (Creixell *et al.*, 2006). In site CT02, the AMS ellipsoids, which vary between weakly prolate and weakly oblate, show well clustered magnetic axes K_1 , K_2 and K_3 .

The magnetic lineation plunges to the SW and the magnetic foliation planes trend NE-SW, being both perpendiculars to the dike trend (dike orientation: $313^\circ/83^\circ$ SW, Fig. 8). A possible explanation is an interchange of the position of magnetic axes, caused by the presence of inverse AMS fabrics that are a relatively common feature of low K_m mafic rocks, in which single-domain magnetite is the dominant magnetic phase (*e.g.*, Ferré, 2002). This hypothesis is supported because magnetite occurs as fine-grained crystals (5 to 80 μ m) in samples of this site.

Unlike CMDS and CrMDS dikes, ETDS dikes do not have oblique asymmetrical AMS fabrics. In most cases, magnetic lineation and magnetic foliation planes tend to be parallel to the dike walls and are interpreted to reflect magma flow, where flow vectors are near vertical (upward) in the central part of the dike swarm (at Punta del Tralca) and SE- and NW-directed at El Tabo and north of Punta del Tralca, respectively, away from the central part of the swarm (Creixell *et al.*, 2009).

5.2. Magnetic properties and AMS ellipsoids of Laguna Verde diorites

In both sites from Laguna Verde (LV01 and LV02), demagnetization temperatures near 560° C and IRM experiments with saturation of magnetic

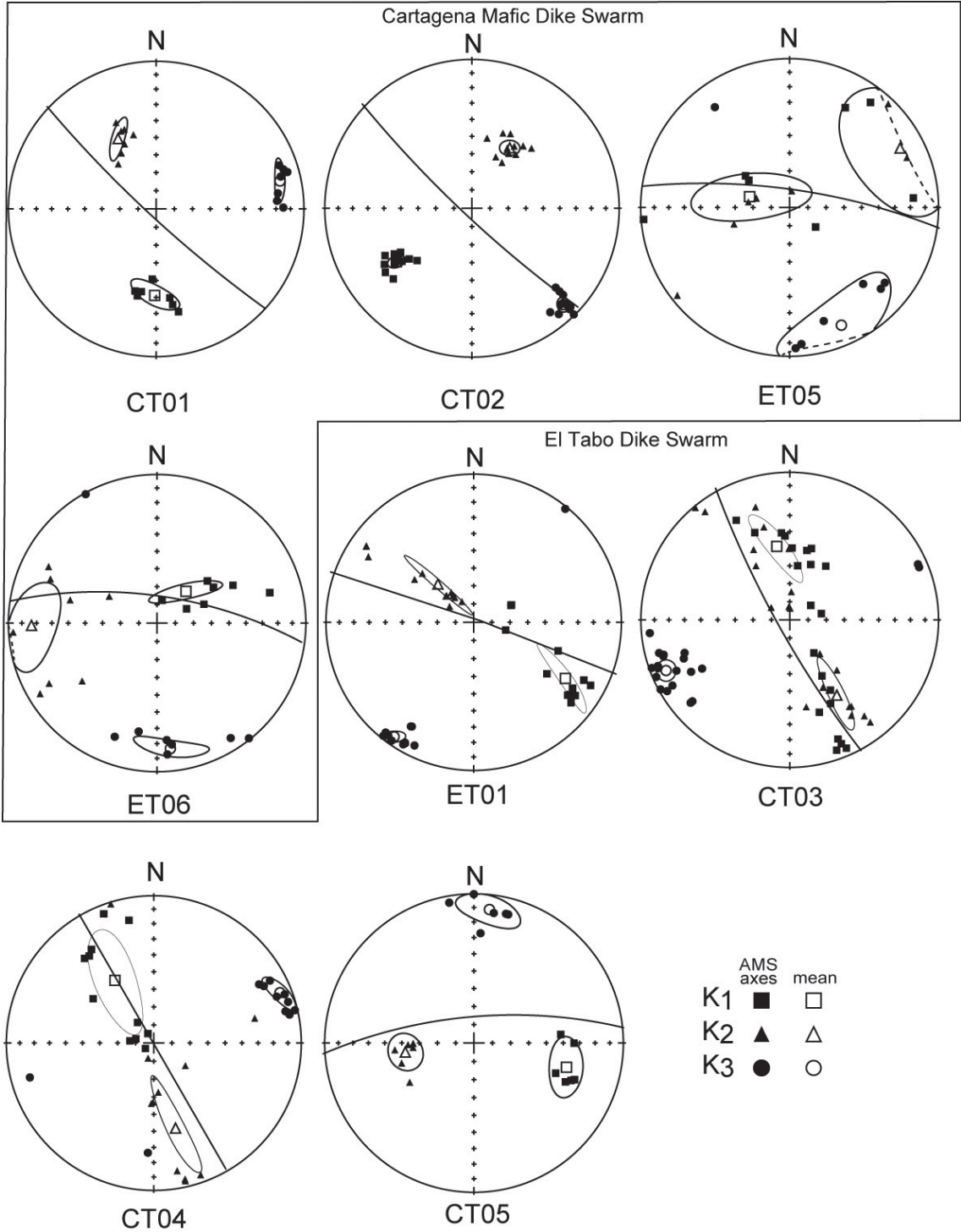


FIG. 8. AMS stereoplots (lower hemisphere projection) of magnetic ellipsoids of mafic dikes of CrMDS (CT01, CT02, ET05 and ET06) and ETDS (ET01, CT03, CT04 and CT05), including 95% confidence cone for each mean magnetic axis ($K1 > K2 > K3$). Solid lines represent dike orientation.

residual near 180 mT suggest that magnetite is the main ferromagnetic phase that controls the AMS signal of the samples (Fig. 7b). Site LV01 of Laguna Verde (Playa Chica) shows weak ferromagnetic behavior (619 to 1374x10⁻⁶ [SI]), in contrast with high K_m values of site LV02 (4490 to 81960x10⁻⁶ [SI], Fig. 9a). In site LV01 there is no clear correlation between K_m and %P' (Fig. 9a) but this correlation is more clear in site LV02, where %P' is higher (>15%, with a mean of 46%). In site LV01 most AMS ellipsoids are oblate. In LV02 prolate ellipsoids are dominant, and shape parameter tend to be well correlated with %P' (Fig. 9b).

The AMS orientation differs between the sites. LV01 show well-clustered AMS axes, with WNW-striking magnetic foliation planes (mean of 305°/87°N) and steeply SE-plunging K_1 magnetic lineation (Fig. 10). In site LV02, the dominant prolate ellipsoids have magnetic lineation plunging to the SW. Magnetic foliation planes strike NNW-SSE, with a mean of 170°/48°W. In general terms, the AMS directional and shape (T) data are well correlated with structures measured in the field (foliation and lineation, Fig. 2f).

6. Geothermobarometry

Composition of minerals used for geothermobarometry is given in table 3 (supplementary data). For Laguna Verde diorites, temperatures estimated using the hornblende-plagioclase geothermometer of Holland and Blundy (1994) give results between 640° and 694°C, consistent with ductile deformation observed in these rocks. Semiquantitative geothermobarometry formulated for mafic rocks, based on TiO₂ and Al₂O₃ contents of amphibole (Ernst and Liu, 1998) can be applied in these rocks, because the mafic/intermediate whole-rock composition and the presence of quartz and a Ti-saturated phase (titani- te). The Ernst and Liu (1998) geothermobarometry method gives temperatures between 700° and 770°C and pressures between 4.8 and 7.6 kbar for amphibole rims. The same method applied to amphibole cores gives temperatures between 730° and 795°C and pressures between 3.5 and 4.8 kbar. As evident from these calculations, pressure results are largely variable in these rocks, and therefore are considered as poorly constrained. Previous results in Jurassic granitoids vary widely between 3.5 and 6.5 kbar (Araneda, 1999). Gana and Tosdal (1996) reported

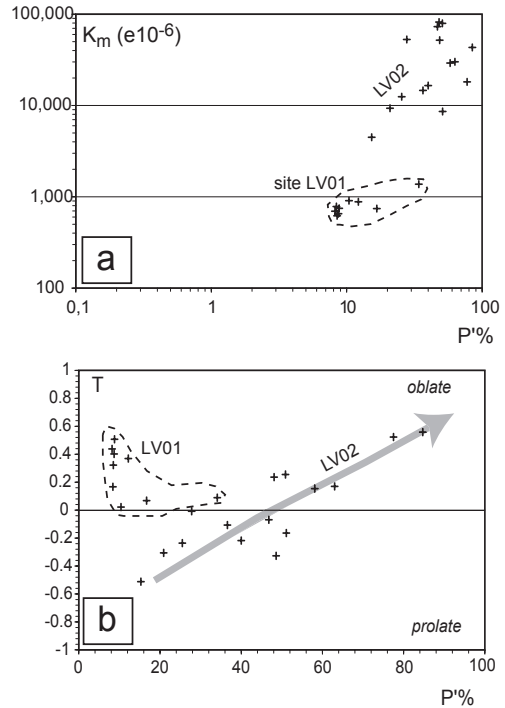


FIG. 9. **a.** Bulk magnetic susceptibility (K_m) versus magnetic anisotropy degree (%P') in samples from Laguna Verde diorites, **b.** Shape parameter (T) versus magnetic anisotropy degree (%P') in the same samples, showing good correlation between these parameters in site LV02.

hornblende crystallization pressures between 4.1 and 5.4 kbar for Middle Jurassic granitoids, located directly to the east of Laguna Verde diorites. The same authors reported lower pressures, between 2.8 and 3.6 kbar, for Upper Jurassic units located to the east. These eastern units are younger than Laguna Verde and Sauce units (Gana and Tosdal, 1996).

Crystallization temperatures in mafic dikes were calculated using compositions of hornblende-plagioclase pairs, with the calibration of Holland and Blundy (1994). Groundmass tschermakitic amphibole from the CrMDS dikes (Fig. 11a), yields temperature estimates between 768° and 819°C, probably corresponding to solidus temperatures, whereas probable solidus pressures (for the same amphiboles), estimated using semiquantitative geobarometer of Ernst and Liu (1998) varies between 3.1 and 5.5 kbar, reflecting the important variability in Si and Al content of these amphiboles (Figs. 11a and 11b).

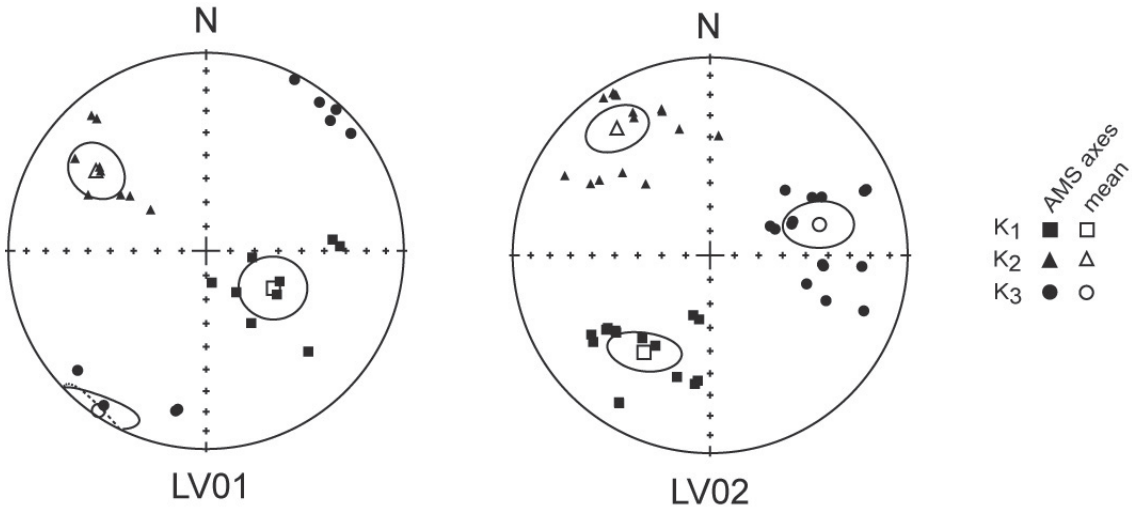


FIG. 10. AMS stereoplots (lower hemisphere projection) of magnetic ellipsoids of Laguna Verde diorites (LV01 and LV02), including 95% confidence cone for each mean magnetic axis ($K_1 > K_2 > K_3$).

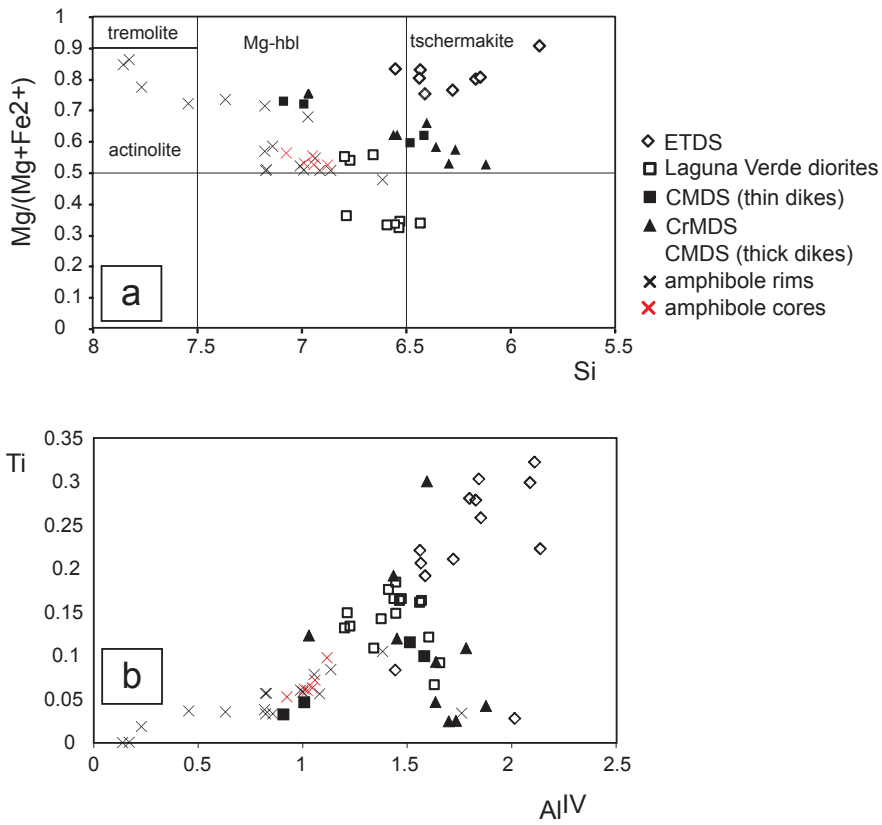


FIG. 11. **a.** Amphibole classification diagram (Leake *et al.*, 1997) based on $Mg/(Mg+Fe^{2+})$ versus Si content (atoms per formula unit), for amphiboles with atomic content $Ca_B > 1.5$ and $(Na+K)_A < 0.5$; **b.** Variation diagram of Ti versus Al^{IV} (atoms per formula unit) in amphiboles from dikes and Laguna Verde diorites.

TABLE 3. REPRESENTATIVE COMPOSITIONS OF AMPHIBOLE AND PLAGIOCLASE FROM MAFIC DIKES AND JURASSIC DIORITES.

Simple Unit	amphibole		plagioclase														
	CC-03-66 Cr:MDS	border	CC-03-66 Cr:MDS	center	CC-03-01 CMDS(1)	border	CC-03-07 CMDS(2)	center	CC-03-52 LV	border	CC-03-48 LV	center	CC-03-52 LV	border	CC-03-07 CMDS(2)	center	
mineral zone																	
SiO ₂	42.64	48.51	49.65	41.89	44.52	42.34	44.41	42.41	44.52	44.52	42.34	44.41	44.52	44.52	63.35	63.28	55.07
TiO ₂	0.42	0.30	0.30	1.39	1.17	1.43	2.55	2.55	1.17	1.17	1.43	2.55	1.17	1.17	0.00	0.03	0.03
Al ₂ O ₃	10.92	5.96	6.40	10.65	9.82	10.34	12.08	12.08	9.82	9.82	10.34	12.08	9.82	9.82	22.80	23.47	28.42
FeO	19.70	18.14	13.96	23.91	15.75	22.95	12.20	12.20	15.75	15.75	22.95	12.20	15.75	15.75	0.16	0.43	0.62
MnO	0.38	0.59	0.23	0.40	0.23	0.41	0.10	0.10	0.23	0.23	0.41	0.10	0.23	0.04	-	-	0.03
MgO	9.72	11.09	14.64	5.95	10.25	6.01	14.06	14.06	10.25	10.25	6.01	14.06	10.25	0.00	0.00	-	0.08
CaO	12.20	11.94	12.65	11.52	11.76	11.36	10.86	10.86	11.76	11.76	11.36	10.86	10.86	4.69	4.72	11.24	11.24
Na ₂ O	1.64	0.76	0.61	1.26	1.04	1.31	2.31	2.31	1.04	1.04	1.31	2.31	1.04	8.28	8.64	4.85	4.85
K ₂ O	0.50	0.49	0.38	1.19	0.98	1.03	0.20	0.20	0.98	0.98	1.03	0.20	0.20	0.44	0.20	0.12	0.12
Total	98.10	97.77	98.84	98.15	95.51	97.16	96.77	96.77	95.51	95.51	97.16	96.77	96.77	99.78	100.77	100.43	100.43
8 O structure																	
Si	6.36	7.18	7.09	6.44	6.77	6.56	6.20	6.20	6.77	6.77	6.56	6.20	6.20	2.81	2.78	2.48	2.48
Ti	0.05	0.03	0.03	0.16	0.13	0.17	0.28	0.28	0.13	0.13	0.17	0.28	0.13	0.00	0.00	0.00	0.00
Al	1.92	1.04	1.08	1.93	1.76	1.89	2.08	2.08	1.76	1.76	1.89	2.08	1.76	1.19	1.22	1.51	1.51
Fe	2.46	2.24	1.67	3.07	2.00	2.97	1.49	1.49	2.00	2.00	2.97	1.49	2.00	0.01	0.02	0.02	0.02
Mn	0.05	0.07	0.03	0.05	0.03	0.05	0.01	0.01	0.03	0.03	0.05	0.01	0.01	0.00	0.00	0.00	0.00
Mg	2.16	2.45	3.12	1.36	2.32	1.39	3.06	3.06	2.32	2.32	1.39	3.06	2.32	0.00	0.00	0.01	0.01
Ca	1.95	1.89	1.94	1.90	1.92	1.88	1.70	1.70	1.92	1.92	1.88	1.70	1.70	0.22	0.22	0.54	0.54
Na	0.47	0.22	0.17	0.38	0.31	0.39	0.66	0.66	0.31	0.31	0.39	0.66	0.31	0.71	0.74	0.42	0.42
K	0.10	0.09	0.07	0.23	0.19	0.20	0.04	0.04	0.19	0.19	0.20	0.04	0.04	0.03	0.01	0.01	0.01
Total cations	15.52	15.22	15.19	15.53	15.44	15.51	15.52	15.52	15.44	15.44	15.51	15.52	15.52	5.01	4.97	4.98	4.98
Fe ³⁺	0.78	0.41	0.53	0.41	0.04	0.24	0.59	0.59	0.04	0.04	0.24	0.59	0.04	-	-	-	-
Fe ²⁺	1.67	1.83	1.14	2.66	1.96	2.74	0.90	0.90	1.96	1.96	2.74	0.90	0.90	0.23	0.23	0.56	0.56
Aliv	1.64	0.82	0.91	1.56	1.23	1.44	1.80	1.80	1.23	1.23	1.44	1.80	1.23	0.74	0.76	0.44	0.44
Alvi	0.28	0.22	0.17	0.37	0.53	0.45	0.28	0.28	0.53	0.53	0.45	0.28	0.28	0.01	0.01	0.01	0.01
Mg/(Mg+Fe ²⁺)	0.56	0.57	0.73	0.34	0.54	0.34	0.77	0.77	0.54	0.54	0.34	0.77	0.77	-	-	-	-

In CMDS, amphibole composition from thick dikes varies largely. In spite that some retrograde actinolitic amphibole has been detected, most of them correspond to Mg-hornblende (Fig. 11a). Amphibole from thin dikes tends to be slightly enriched in Ti and Mg than those from thick dikes (Figs. 11a, b).

In thin dikes of the CMDS, crystallization temperatures for hornblende vary between 683° and 715°C. In thick dikes of CMDS, crystallization temperatures for hornblende-plagioclase rim compositions vary between 620° and 690°C. Temperatures for core compositions of hornblende-plagioclase pairs are consistently higher, varying between 724°-771°C, representing magmatic equilibrium temperatures. These amphibole cores have a slight tendency to show higher Ti contents than amphibole rims (Fig. 11b). Pressure estimates using Ernst and Liu (1998) geobarometer, are indistinguishable between rims and core compositions of amphiboles and vary between 2 and 4.7 kbar.

Brown amphiboles from NW-striking dikes of the ETDS are characterized by the highest Mg/(Mg+Fe²⁺) ratios and Ti contents (Figs. 11a and 11b), and consistently with it, the magmatic temperatures estimated are also high, between 790° and 910°C, using the geothermometer of Otten (1984). Estimations with the geothermobarometer of Ernst and Liu (1998) yield temperatures around 850°C and pressure of crystallization between 2.8 and 3 kbar.

7. Discussion

7.1. Significance of shape and AMS fabrics of dike swarms: insights into emplacement mechanisms

Microscopic examination of selected samples of dikes allows recognizing magnetite as isolated (locally elongated) grains from each other in the groundmass of these rocks. This suggests, in conjunction with K_m values of the samples, that AMS is controlled by shape anisotropy of magnetite. Where field structures are well observed, *e.g.*, in Laguna Verde diorites and CMDS, a correlation between AMS and shape fabrics is clearly documented, and then AMS fabrics are a good proxy of the orientation of the finite strain ellipsoid of the rocks.

7.1.1. Emplacement under transtension in CMDS and CrMDS

Thick dikes of the CMDS show abundant evidences of ductile deformation of crystals at microscopic scale, however, some dikes also show a well developed magmatic microfabric, not affected by solid-state recrystallization. Evidences for ductile deformation presented by Creixell *et al.* (2006) and in this work, mostly show that the dike matrix is affected by important dynamic recrystallization including grain-size reduction (Figs. 3a, b). Beside this, internal fractures of plagioclase phenocrysts are filled by magmatic minerals (mostly hornblende and oligoclase), suggesting the presence of fluid during fracturing and deformation (*e.g.*, Bouchez *et al.*, 1992). The coexistence in equilibrium of high-temperature ductile deformation and fractures filled by a possible melt suggests that the microfabrics register the strain occurred from the submagmatic state to high-temperature solid state deformation. We consider submagmatic deformation as the ductile strain occurred in the presence of proportion of residual melt below the necessary to allow magmatic flow (Paterson *et al.*, 1989). These observations are in agreement with temperature estimates between 620° and 690°C that are close to slightly below solidus for intermediate compositions (Piwinskii, 1968; Huang and Wyllie, 1986; Schmidt, 1993).

Inside this deformed matrix of the thick dikes of CMDS, magnetite occurs as isolated grains surrounded by titanite rims (Fig. 3b). The magnetite grains are oriented and elongated following the deformation of the groundmass. These textural arrangements imply that: **a.** AMS fabrics, developed by the presence of magnetite, are controlled by the shape anisotropy of this mineral rather than distribution anisotropy. This is consistent with the good correspondence between AMS and shape fabrics of dikes (Creixell *et al.*, 2006); **b.** the AMS fabrics, and then the asymmetrical pattern they represent, are representative of the shape fabric of the dikes, specifically the fabric of the deformed matrix. Because the matrix was deformed in the submagmatic state (ductile deformation in the presence of small amount of melt), the asymmetrical fabric was acquired mainly in the late stage of crystallization of the dikes, probably close to emplacement. In the case of CrMDS dikes from Panul, that exhibit magmatic textures and temperature estimations

>700°C, acquisition of asymmetrical fabric occurred during magmatic crystallization.

Thick dikes of CMDS and dikes of CrMDS from Panul area (Fig. 1c) have asymmetrical magnetic fabrics, with near-vertical foliations clockwise oblique to dike walls, and shallow plunging magnetic lineations. At dike margins, the magnetic foliation in most cases is parallel to dike walls. Following the models of Blumenfeld and Bouchez (1988), Hutton (1992) and Correa-Gomes *et al.* (2001), this pattern of fabric reflects the effects of sinistral deformation along dike walls during emplacement and also indicates that the influence of magma flow dynamics was minor on fabric development.

To understand the meaning of the low-plunging lineations in the studied dikes, these magmatic bodies need to be considered as dike-shear zones, taking into account that sinistral deformation was fundamental in fabric development and took place during or close to its emplacement (*e.g.*, dikes were emplaced along active sinistral fractures). Theoretical models of lineation development in shear zones (Tikoff and Greene, 1997; Teyssier and Tikoff, 1999) predict that near-horizontal lineations with vertical foliations are produced during

both transtension and transpression, depending on the magnitudes of pure and simple shear and the orientation of the shear zone with respect to the external deformation field. Specifically, fabrics characterized by vertical foliations and horizontal lineations can be originated by deformation dominated by simple over pure shear, as suggested in the previous paragraphs, or by deformation that registered a low cumulative strain (Teyssier and Tikoff, 1999). We have not enough data to discriminate more exactly between these mechanisms. In spite of this, for the thick dikes of the CMDS and the CrMDS, the sinistral deformation fabric was developed during or close to emplacement implying that the left-lateral movement was coetaneous with a component of horizontal dilation along the host fractures, needed to accommodate the dike thicknesses, that cumulatively represents around 3.5 km of extension (Creixell, 2007). This occurrence of coetaneous sinistral displacement and horizontal dilation across the host fractures indicates that the dikes were emplaced during sinistral transtension. Finally, if the magnetic lineations are representative of stretching during fabric acquisition, they indicate oblique opening in NNW-SSE direction

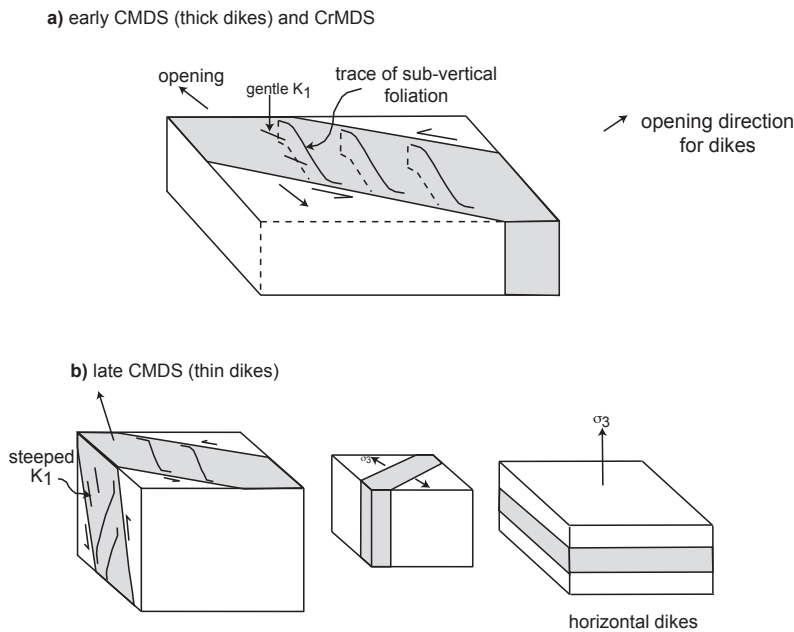


FIG. 12. **a.** Schematic cartoons of dike emplacement for thick dikes of CMDS and CrMDS, and **b.** Thin dikes of CMDS and horizontal dikes of CMDS and CrMDS.

(Fig. 12a), consistent with some field evidence of oblique opening of dikes (section 4.4).

7.1.2. Emplacement under transpression in CMDS, CrMDS and Laguna Verde diorites

Thin dikes of CMDS are characterized by magmatic fabrics, without evidence of solid state deformation. Dikes of the CrMDS from Punta Suspiro show local evidence of high-temperature solid-state fabrics that will be explained in detail below. In the same way as observed in thick dikes of the CMDS, in all these dikes magnetite occurs as isolated grains in the ground-mass, in intergrowth relation with silicate minerals, suggesting that the AMS ellipsoid is controlled by the orientation of these magnetite grains and could be representative of the rock fabric.

The AMS fabrics of thin dikes of the CMDS are asymmetrical, with magnetic foliation clockwise oblique to dike trend, with a pattern indicative of sinistral shear (*e.g.*, Blumenfeld and Bouchez, 1988; Hutton, 1992; Correa-Gomes *et al.*, 2001), but steeply-plunging lineations are dominant. Dikes from Punta Suspiro are characterized by steeply dipping magnetic foliation and also steeply-plunging magnetic lineations. High plunge of magnetic lineations in shear zones are developed under transpression (Tikoff and Greene, 1997; Teyssier and Tikoff, 1999). If we consider these dikes as emplaced along active shear fractures, as evidenced by AMS fabrics, an important component of horizontal shortening was associated to their emplacement. Indeed, this horizontal shortening is evidenced by **a.** field indicators of reverse shearing along dike walls in vertical sections (Creixell *et al.*, 2006) and **b.** occurrence of subhorizontal thin dikes of the CMDS and CrMDS (Fig. 5c, d). These horizontal dikes are interpreted as a product of near vertical dilation and therefore a component of shortening in the horizontal plane (Fig. 12b). Horizontal shortening is also deduced from near-vertical mafic dikes of the CrMDS from Punta Suspiro that are displaced by E-W striking reverse shear zones (Fig. 5a). These reverse shear zones mostly show fragile deformation, but these dikes are deformed in highly ductile conditions where they are cut by these faults, suggesting that reverse activity of these faults occurred shortly after dike emplacement.

In the coeval Laguna Verde diorites, we have not enough detailed data to reconstruct the history of emplacement and deformation of these rocks, but the registered ductile structures are characterized

by NW-SE sinistral shear zones with near-vertical foliation and steeply-plunging lineations (site LV01 and Fig. 2f) and coeval folds with horizontal axes and reverse shear zones. The microfabrics and geothermometry suggest that deformation occurred at high temperature below solidus.

Finally, the combination of sinistral shear along NW-SE striking structures occupied by dikes and diorites, with a coeval component of horizontal shortening, indicate that emplacement and deformation of thin dikes of the CMDS, CrMDS dikes from Punta Suspiro and Laguna Verde diorites occurred in a regime of sinistral transpression.

7.1.3. Fabrics and emplacement of ETDS

Two perpendicular sets of dikes were recognized in the ETDS. Dike-parallel joints and chlorite-epidote veins cut by dikes are evidence of emplacement at shallow depth. Since these structures are not widespread at regional scale, they probably were directly associated to dike emplacement. The presence of dike-parallel joints in dikes has been described as evidence of dike propagation as self-generated fractures, where these joints were caused by tensile stress produced near and away from propagating dike tip (Delaney *et al.*, 1986). This implies that the dikes were emplaced along tensional fractures, perpendicular to the least principal stress direction (σ_3). Consistently with this hypothesis, we can observe that the homogeneous orientation of each dike set in the ETDS does not follow the variation in fabric orientation of the country rock (Figs. 2g to 2i), and therefore, emplacement of such dikes was not controlled by the country rock fabrics, at least at the exposed crustal level. Also, passive markers observed mostly at Punta de Tralca suggest that opening occurred normal to dike walls (Figs. 6c to 6f), as expected for tensional fracturing or tension gashes (*e.g.*, Anderson, 1951; Emerman and Marrett, 1990).

Taking these observations into account, the presence of two nearly coeval and perpendicular dike systems in the ETDS indicates two directions of crustal dilation. Horizontal radial extension cannot account as a mechanism that explains the emplacement of ETDS, simply because radial extension (with vertical maximum stress axis σ_1) produces radial sets of dikes or fractures. A more possible tensional regime is that each dike generation was associated to changes in the stress pattern, with interchange of σ_2 and σ_3 during emplacement of each dike generation (with $\sigma_2 \sim \sigma_3$ lying

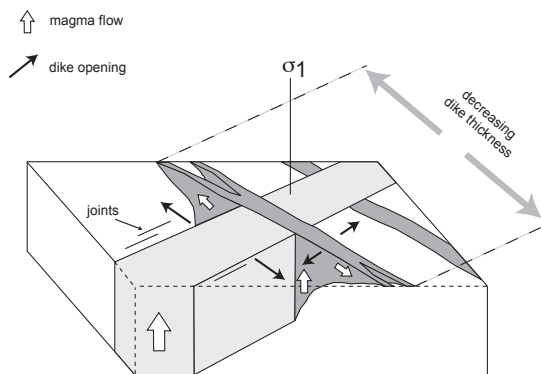


FIG. 13. Schematic cartoon of dike emplacement for ETDS. Magma flow directions (white arrows) as determined by AMS fabrics by Creixell *et al.* (2009). Opening direction of dikes determined by field data. Minimum principal stress direction (σ_1) is near vertical.

in the horizontal plane, Fig. 13). A possible explanation for this model is that the pressure imposed by magma intrusion allows inversion of horizontal stress axes at the local scale. This is possible if differential stress in the horizontal plane is sufficient small to be modified by the intrusion of dikes. This mechanism could be efficient for this kind of minor intrusions, such as the ETDS, at shallow crustal levels. A similar mechanism was proposed by Vigneresse *et al.* (1999) to explain inversion of vertical and horizontal stress axes in a tensional regime associated with magma intrusion.

The area of higher dike density and lower dike spacing in NW-striking dikes coincides with vertical magma flow vectors determined from the AMS (Creixell *et al.*, 2009), and probably corresponds to the central portion of the swarm. Away from it, magma flow vectors become gently-plunging and dike density decreases (Fig. 13).

7.2. Geodynamic and tectonic setting of emplacement of dike swarms

7.2.1. CMDS and CrMDS: Middle-Late Jurassic change from transtension to transpressional deformation and associated compositional variations of magmas

From the data and discussion presented in the previous sections, we envisage two distinct regimes of magma emplacement that were active during Middle-Late Jurassic times in the area. A first regime of sinistral transtension across NW-SE to WNW-ESE

structures was followed by sinistral transpression along similar fracture systems. Abundant field data supports this sequence of deformation in the area:

a. In CMDS, thick dikes, emplaced under transtension, are systematically intruded by thin dikes, emplaced in transpression.

b. In CrMDS, reverse faults postdate dike emplacement.

c. Horizontal dikes are everywhere associated with dikes emplaced in transpression.

This temporal sequence of deformation implies that host fractures of dikes quickly change their tectonic behavior between 163 and 157 Ma. This change is correlated with important compositional variations observed in the dike swarms. Dikes emplaced during transtension (*e.g.*, thick dikes of CMDS) have an enriched geochemical signature (high Ti, Nb, Zr and other incompatible elements) with respect to dikes emplaced during transpression, that show a more primitive signature, with higher MgO, Cr and Ni (Creixell *et al.*, 2009). These changes are also accompanied by variations in magnetic mineralogy, where the first group of dikes is dominated by the presence of low-Ti magnetite and dikes emplaced in transpression contain magnetite and sulphide phases, such as pyrrhotite and pyrite. This implies that the changing tectonic behavior of structures promoted magma extraction from different reservoirs, where more primitive magmas ascend through dikes during transpressive deformation, probably associated to higher magma overpressures.

7.2.2. Emplacement and compositional variations in ETDS

The field and AMS data on the ETDS indicate that both NE and NW-striking dike sets were emplaced along self-generated tensile fractures. As discussed above, the emplacement of these dike sets occurred in successive stages of modification of the stress field. As in the Jurassic dike swarms, structural variations in different dike sets are correlated with compositional changes. NE-striking dikes are Ti-enriched, whereas NW-striking dikes are comparatively poorer in Ti and other elements such as Nb, Zr and REE (Creixell *et al.*, 2009). Another difference is that NE-striking dikes are systematically thicker than NW-striking dikes (section 4. and Fig. 13). According to recent results in mafic dike swarms in Greenland (Klausen and Larsen, 2002) and in the Deccan Traps (Ray *et al.*, 2007), differences in dike thickness can be con-

trolled by the depth of magma reservoirs, but also by differences in magma viscosity (Wada, 1994), where deeper reservoirs or also more viscous magmas can produce thicker dikes. Since major elements geochemistry and therefore magma viscosity is not dramatically different between NE and NW-striking dikes, we suggest that differences in dike thickness are controlled by injection of magmas from reservoirs located at different depths.

7.3. Regional implications

7.3.1. Changes in the axis of the Coastal Batholith

The current results give preliminary insights into the tectonic evolution of the Mesozoic magmatic arc of central Chile. The structures observed in the dike swarms and diorites show that the evolution of this western part of the batholith took place in several stages.

At a regional scale from north to south between 33° and 34°S, the axis of the Middle-Upper Jurassic coastal batholith changes from *ca.* N-S to NW-SE, coincident with the close occurrence of NW-SE structures crossing the Coastal Cordillera (Fig. 1b). The current results suggest that magma ascent in the batholith, marked by the presence of the dike swarms, have been controlled by NW-SE structures, at least during the first stages of growth of the batholith (163-157 Ma). As a preliminary hypothesis, we propose that these structures controlled and focused the emplacement of Middle-Upper Jurassic plutons in the area, to the east of the dike swarms and caused the change in the axis of the batholith to a NW-SE orientation. In contrast, this change in the orientation of the plutonic belt is not observed in Lower Cretaceous plutons, that are distributed continuously along a N-S belt in the eastern slope of the Coastal Range of central Chile (SERNAGEOMIN, 2002). Detailed fabric studies in one of these plutons (Caleu pluton) do not detect the influence of oblique (NW-striking) structures in its emplacement (Parada *et al.*, 2002). This is a preliminary suggestion that the NW-SE structures of the area were more active during the Middle-Late Jurassic.

7.3.2. Implications for the evolution of NW- to WNW-trending lineaments of central Chile

Several authors note the presence of important NW-SE to WNW-ESE structures oblique to the Andean orogen (*e.g.*, Glodny *et al.*, 2008), that are distributed along most of the central and southern

Andes, but have an outstanding density in the 33°-34°S segment, coincident with the transition between the 'flat-slab' segment to the north and the southern volcanic zone to the south (*e.g.*, Yáñez *et al.*, 2001, among others). These structures control the evolution of volcano-tectonic basins during the Cenozoic as transtensional and probably normal faults (Wall *et al.*, 1996; Rivera and Cembrano, 2000). Our current results, combined with observations made by Godoy and Loske (1988) indicate that these large Cenozoic structures are inherited from structures that are at least as old as Middle Jurassic that hosted and deformed the mafic dike swarms and diorites studied here. Indeed, the western end of most of the main NW to WNW-striking lineaments between 33° and 33°45'S coincides with the localization of the dike swarms studied here or with the contact between Jurassic and Late Paleozoic intrusions.

8. Concluding remarks

Field data and AMS fabrics indicate that the CMDS and CrMDS were emplaced in two stages, a first sinistral-transtension, followed by sinistral transpression. The transpressive structures are also observed in the Middle-Upper Jurassic Laguna Verde diorites which show evidence of ductile deformation close to its emplacement. The changes in deformation kinematics were associated with compositional changes in the mafic dikes, with the more primitive magmas emplaced during the transpressive stage. This suggests extraction of magmas from different reservoirs during each deformation event.

The Lower Cretaceous mafic dikes (ETDS) were emplaced along tensional structures, with different dike orientations (NW- and NE-striking mafic dikes) associated to different composition and thicknesses of dikes, pointing again to extraction of magmas from different reservoirs, related to low and high-Ti basaltic magmas.

Finally, a general framework for the tectonic evolution of the Jurassic magmatic arc of central Chile has been envisaged here, with different styles of deformation in several stages. The current results suggest that occurrence of NW- to WNW-trending lineaments played a fundamental role in the emplacement and deformation of Middle-Upper Jurassic dike swarms during the first stages of growth of the Jurassic batholith between 33° and 34°S. The current results, in addition to previous works, suggest that

these regional scale oblique structures that crosscut the Andes between 33° and 33°45'S were inherited in part from Jurassic structures, which were reactivated during the Cenozoic.

9. Acknowledgments

This research was funded by Fondecyt N°1031000 (D.M.) and was a part of the Ph.D. Thesis of the first author, carried out with financial assistance from MECESUP and CONICYT grants. Microprobe analyses at Zelmi Laboratory were financed by TU-Berlin and a DAAD studentship for the first author. These analyses were performed under guidance of Prof. G. Franz. The authors want to thank R. Santelices, C. Valenzuela, M. Calderón, N. Astudillo and M. Belmar for sharing with us some days in the field. The authors also want to thank J. Vargas for assistance in mineral separation and F. Galbert and I. Preuss for assistance with microprobe analyses at Zelmi Laboratory, TU-Berlin. J. Cembrano, F. Hervé and C. Mpodozis made valuable comments on early versions of the manuscript. This paper was substantially improved by the reviews made by J. Bartley, A. Willner and H. Diot.

10. References

- Anderson, E.M. 1951. The dynamics of faulting. Oliver and Boyd: 206 p. Edinburgh.
- Aguirre, L.; Féraud, G.; Morata, D.; Vergara, M.; Robinson, D. 1999. Time interval between volcanism and burial metamorphism and rate of basin subsidence in a Cretaceous Andean extensional setting. *Tectonophysics* 313: 433-447.
- Arancibia, G.; Matthews, S.; Pérez de Arce, C. 2006. K-Ar and ⁴⁰Ar/³⁹Ar geochronology of supergene processes in Atacama Desert, northern Chile: tectonic and climatic relations. *Journal of the Geological Society of London* 163 (1): 107-118.
- Araneda, E. 1999. Características geoquímicas y variaciones termobarométricas en el Batolito de la Costa de Chile Central entre los 33° y 33°45'S. Memoria de Título (Unpublished), Universidad de Chile, Departamento de Geología: 89 p.
- Arce, M. 2002. Condiciones de formación y naturaleza de las estructuras del complejo plutónico Santo Domingo, V Región: evidencias de terreno y de fábricas magnéticas. Memoria de Título (Unpublished), Universidad de Chile, Departamento de Geología: 80 p.
- Blumenfeld, P.; Bouchez, J.L. 1988. Shear criteria in granite and migmatite deformed in the magmatic and solid states. *Journal of Structural Geology* 10 (4): 361-372.
- Bouchez, J.L.; Delas, C.; Gleizes, G.; Nédélec, A.; Cuney, M. 1992. Submagmatic microfractures in granites. *Geology* 20: 35-38.
- Cembrano, J.; González, G.; Arancibia, G.; Ahumada, I.; Olivares, V.; Herrera, V. 2005. Fault zone development and strain partitioning in an extensional strike-slip duplex: A case study from the Mesozoic Atacama fault system, Northern Chile. *Tectonophysics* 400: 105-125.
- Clemente, C.S.; Amorós, E.B.; Garcés Crespo, M. 2007. Dike intrusion under shear stress: effects on magnetic and vesicle fabrics in dikes from rift zones of Tenerife (Canary Islands). *Journal of Structural Geology* 29: 1931-1942.
- Correa-Gomes, L.C.; Souza Filho, C.R.; Martins, C.J.F.N.; Oliveira, E.P. 2001. Development of symmetrical and asymmetrical fabrics in sheet-like igneous bodies: the role of magma flow and wall-rock displacements in theoretical and natural cases. *Journal of Structural Geology* 23: 1415-1428.
- Corvalán, J.; Munizaga, F. 1972. Edades radiométricas de rocas intrusivas y metamórficas de la Hoja Valparaíso-San Antonio. Instituto de Investigaciones Geológicas, Boletín 28: 28 p. Santiago.
- Cordani, U.; Munizaga, F.; Hervé, F.; Hervé, M. 1976. Edades radiométricas provenientes del basamento cristalino de la Cordillera de la Costa de las provincias de Valparaíso y Santiago. *In Congreso Geológico Chileno*, No. 1, Actas 2: F213-F222. Santiago.
- Creixell, C. 2007. Emplazamiento y petrogénesis de enjambres de diques máficos de Chile central (30°-33°45'S): implicancias tectónicas en el desarrollo del arco Jurásico-Cretácico Temprano. Ph.D. Thesis (Unpublished), Universidad de Chile: 275 p.
- Creixell, C.; Parada, M.A.; Roperch, P.; Morata, D.; Arriagada, C.; Pérez de Arce, C. 2006. Syntectonic emplacement of the Middle Jurassic Concón Mafic Dike Swarm, Coastal Range, central Chile (33°S). *Tectonophysics* 425: 101-122.
- Creixell, C.; Parada, M.A.; Morata, D.; Roperch, P.; Arriagada, C. 2009. The genetic link between mafic dike swarms and plutonic reservoirs in the Mesozoic of central Chile (30°-33°45'S): insights from AMS and geochemistry. *International Journal of Earth Sciences* 98: 177-201.
- Delaney, P.T.; Pollard, D.D.; Ziony, J.; McKee, E.H. 1986. Field relations between dikes and joints: emplacement processes and paleostress analysis. *Journal of Geophysical Research* 91: 4920-4938.
- Emerman, S.; Marrett, R. 1990. Why dikes? *Geology* 18: 231-233.

- Ernst, W.G.; Liu, J. 1998. Experimental phase-equilibrium study of Al- and Ti-contents of calcic amphibole in MORB- A semiquantitative thermobarometer. *American Mineralogist* 83: 952-969.
- Féménias, O.; Diot, H.; Berza, T.; Gauffriau, A.; Demaiffe, D. 2004. Asymmetrical to symmetrical magnetic fabric of dikes: paleo-flow orientations and paleo-stresses recorded on feeder-bodies from the Motru Dike Swarm (Romania). *Journal of Structural Geology* 26: 1401-1418.
- Ferré, E. 2002. Theoretical models of intermediate and inverse AMS fabrics. *Geophysical Research Letters* 29(7): 4 p.
- Gana, P.; Tosdal, R. 1996. Geocronología U-Pb y K-Ar en intrusivos del Paleozoico y Mesozoico de la Cordillera de la Costa, Región de Valparaíso, Chile. *Revista Geológica de Chile* 23 (2): 151-164.
- Gana, P.; Wall, R.; Gutiérrez, A. 1996. Mapa geológico del área de Valparaíso-Curacaví. Servicio Nacional de Geología y Minería, Mapas Geológicos 1, escala 1: 100.000.
- Glazner, A.; Bartley, J.; Carl, B. 1999. Oblique opening and noncoaxial emplacement of the Jurassic Independence dike swarm, California. *Journal of Structural Geology* 21 (10): 1275-1283.
- Godoy, E.; Loske, W. 1988. Tectonismo sinplutónico de dioritas jurásicas al sur de Valparaíso: datos U-Pb sobre la Fase Quintay. *Revista Geológica de Chile* 15 (2): 119-127.
- Glodny, J.; Echtler, H.; Collao, S.; Ardiles, M.; Burón, P.; Figueroa, O. 2008. Differential Late Paleozoic active margin evolution in South-Central Chile (37°S-40°S)-the Lanahue Fault Zone. *Journal of South American Earth Sciences* 26: 397-411.
- Grocott, J.; Brown, M.; Dallmeyer, R.D.; Taylor, G.K.; Treloar, P.J. 1994. Mechanisms of continental growth in extensional arcs: an example from the Andean plate-boundary zone. *Geology* 22: 391-394.
- Grocott, J.; Taylor, G.K. 2002. Deformation partitioning, magmatic arc fault systems and the emplacement of granitic complexes in the Coastal Cordillera, north Chilean Andes (25-27°S). *Journal of Geological Society of London* 159: 425-442.
- Hervé, F. 1976. Petrografía del basamento cristalino en el área Laguna Verde-Quintay, Provincia de Valparaíso, Chile. In *Congreso Geológico Chileno*, No. 1, Actas: F125-F143. Santiago.
- Hervé, F.; Munizaga, F.; Parada, M.A.; Brook, M.; Pankhurst, R.; Snelling, N.; Drake, R. 1988. Granitoids of the Coast Range of central Chile: geochronology and geologic setting. *Journal of South American Earth Sciences* 1: 185-194.
- Holland, T.; Blundy, J. 1994. Non-ideal interactions in calcic amphiboles and their bearing on amphibole-plagioclase thermometry. *Contributions to Mineralogy and Petrology* 116: 433-444.
- Huang, W.L.; Wyllie, P.J. 1986. Phase relationships of gabbro-tonalite-water at 15 kbar with applications to differentiation and anatexis. *American Mineralogist* 71: 301-316.
- Hutton, D. 1992. Granite sheeted complexes: evidence for the dyking ascent mechanism. *Transactions of the Royal Society of Edinburgh: Earth Sciences* 83: 377-382.
- Irwin, J.; Sharp, W.; Spangler, R.; Drake, R. 1987. Some paleomagnetic constraints in the tectonic evolution of the coastal cordillera of central Chile. *Journal of Geophysical Research* 92: 3603-3614.
- Jelinek, V. 1981. Characterization of the magnetic fabric of rocks. *Tectonophysics* 79: 63-67.
- Klausen, M.B.; Larsen, H.C. 2002. East Greenland coast-parallel dike swarm and its role in continental breakup. In *Volcanic rifted margins* (Menzies, M.A.; Klempner, S.L.; Ebinger, C.J.; Baker, J.; editors). Geological Society of America Special Paper 362: 137-162. Boulder.
- Leake, B.; Woolley, A.; Arps, C.; Birch, W.; Gilbert, M.C.; Grice, J.; Hawthorne, F.; Kato, A.; Kisch, H.; Krivovichev, V.; Linthout, K.; Laird, J.; Mandarino, J.; Maresch, W.; Nickel, E.; Rock, N.; Schumacher, J.; Smith, D.; Stephenson, N.; Ungaretti, L.; Whittaker, E.; Youzhi, G. 1997. Nomenclature of amphiboles.: Report of the Subcommittee on amphiboles of the International Mineralogical Association, Commission on new minerals and mineral names. *Canadian Mineralogist* 35 (1): 219-246.
- Levi, B. 1973. Eastward shift of Mesozoic and Early Tertiary volcanic centers in the Coast Range of central Chile. *Geological Society of America Bulletin* 84: 3901-3910.
- Martín-Hernández, F.; Dekkers, M.J.; Bominaar-Silkens, I.M.A.; Maan, J.C. 2008. Magnetic anisotropy behaviour of pyrrhotite as determined by low-and high-field experiments. *Geophysical Journal International* 174 (1): 42-54.
- Muñoz Cristi, J. 1964. Estudios petrográficos y petrológicos sobre el Batolito de la Costa de las provincias de Santiago y Valparaíso. Universidad de Chile, Publicación 25: 94 p.
- Otten, M. 1984. The origin of brown hornblende in the Artfjället gabbro and dolerites. *Contributions to Mineralogy and Petrology* 86 (2): 189-199.
- Parada, M.A.; Feraud, G.; Fuentes, F.; Aguirre, L.; Morata, D.; Larrondo, P. 2005. Ages and cooling history of the Early Cretaceous Caleu pluton: testimony of a switch

- from a rifted to a compressional continental margin in central Chile. *Journal of the Geological Society of London* 162: 273-287.
- Parada, M.A.; Larrondo, P.; Guiresse, C.; Roperch, P. 2002. Magmatic gradients in the Cretaceous Caleu pluton (central Chile): injections of pulses from a stratified reservoir. *Gondwana Research* 5: 307-324.
- Parada, M.A.; Nystrom, J.; Levi, B. 1999. Multiple sources for the Coastal batholith of central Chile (31-34°S): geochemical and Sr-Nd isotopic evidence and tectonic implications. *Lithos* 46: 505-521.
- Parada, M.A.; Rivano, S.; Sepúlveda, P.; Hervé, M.; Hervé, F.; Puig, A.; Munizaga, F.; Brook, M.; Pankhurst, R.; Snelling, N. 1988. Mesozoic and Cenozoic plutonic development in the Andes of central Chile (30°30' S-32°30' S). *Journal of South American Earth Sciences* 1: 249-260.
- Paterson, S.R.; Vernon, R.H.; Tobisch, O. 1989. A review of criteria for the identification of magmatic and tectonic foliations in granulites. *Journal of Structural Geology* 11 (3): 349-363.
- Piracés, R. 1976. Estratigrafía de la Cordillera de la Costa entre la Cuesta El Melón y Limache, Provincia de Valparaíso, Chile. *In Congreso Geológico Chileno*, No. 1, Actas 1: A65-A82. Santiago.
- Piwinskii, A.J. 1968. Experimental studies of igneous rock series: Central Sierra Nevada batholith, California. *Journal of Geology* 76: 548-570.
- Ray, R.; Sheth, H.; Mallik, J. 2007. Structure and emplacement of the Nandurbar-Dhule mafic dike swarm, Deccan Traps, and the tectonomagmatic evolution of flood basalts. *Bulletin of Volcanology* 69: 537-551.
- Rivera, O.M.; Cembrano, J. 2000. Modelo de formación de cuencas volcano-tectónicas en zonas de transferencia oblicuas a la cadena andina: el caso de las cuencas oligo-miocenas de Chile central y su relación con estructuras NWW-NW (33°-34°30'S). *In Congreso Geológico Chileno*, No. 9, Actas 2: 631-636. Puerto Varas.
- Scheuber, E.; González, G. 1999. Tectonics of the Jurassic-Early Cretaceous magmatic arc of the north Chilean Coastal Cordillera (22°-26°S): a history of crustal deformation along a convergent plate boundary. *Tectonics* 18 (5): 895-910.
- Schmidt, M.W. 1993. Phase relations and compositions in tonalite as a function of pressure: An experimental study at 650° C. *American Journal of Science* 293: 1011-1060.
- SERNAGEOMIN. 2002. Mapa Geológico de Chile 1:1.000.000. Servicio Nacional de Geología y Minería, Carta Geológica de Chile, Serie Geología Básica 75, 1 mapa en 3 hojas.
- Siña, A. 1987. El Batolito de la Costa entre Algarrobo y Rocas de Santo Domingo (Chile central, 33°30'S): geología e interpretaciones petrogenéticas. *Comunicaciones* 38: 47-66.
- Tarling, H.R.; Hrouda, F. 1993. The magnetic anisotropy of rocks. Chapman and Hall: 217 p.
- Teyssier, Ch.; Tikoff, B. 1999. Fabric stability in oblique convergence and divergence. *Journal of Structural Geology* 21: 969-974.
- Tikoff, B.; Greene, D. 1997. Stretching lineations in transpressional shear zones. *Journal of Structural Geology* 19: 29-40.
- Thomas, H. 1958. Geología de la Cordillera de la Costa entre el valle de La Ligua y la Cuesta de Barriga, Santiago. *Instituto de Investigaciones Geológicas*, Boletín 2: 86 p.
- Vergara, M.; Levi, B.; Nystrom, J.; Cancino, A. 1995. Jurassic and Early Cretaceous island arc volcanism, extension and subsidence in the Coast Range of central Chile. *Geological Society of America Bulletin* 107: 1427-1440.
- Vigneress, J-L.; Tikoff, B.; Améglio, L. 1999. Modification of the regional stress field by magma intrusion and formation of tabular granitic plutons. *Tectonophysics* 302: 203-224.
- Wada, Y. 1994. On the relationship between dike width and magma viscosity. *Journal of Geophysical Research* 99 (B9): 17743-17755.
- Wall, R.; Gana, P.; Gutiérrez, A. 1996. Geología de la Hoja Santiago, área de San Antonio-Melipilla, regiones de Valparaíso, Metropolitana y del Libertador General Bernardo O'Higgins. Servicio Nacional de Geología y Minería, Mapas Geológicos 2, escala 1:100.000.
- Willner, A.; Thomson, S.; Kroner, A.; Wartho, J.; Wijbrans, J.; Herve, F. 2005. Time markers for the evolution and exhumation history of a late Paleozoic paired metamorphic belt in central Chile (34°-35°30'S). *Journal of Petrology* 46: 1835-1858.
- Yáñez, G.; Gana, P.; Fernández, R. 1998. Origen y significado geológico de la Anomalía Melipilla, Chile central. *Revista Geológica de Chile* 25 (2): 175-198.
- Yáñez, G.; Ranero, C.; Von Huene, R.; Díaz, J. 2001. Magnetic anomaly interpretation across the southern central Andes (32-34°S): the role of the Juan Fernández Ridge in the Late Tertiary evolution of the margin. *Journal of Geophysical Research* 106: 6325-6345.